

Chapter 6

Preparation

Obviously, every nanostructure, whether it is a thin film or a laterally structured sample, first has to be prepared in some form. This is an area of science in its own right, and we will see in this Chapter that there is a lot of physics behind the growth and preparation of nanostructures.

Thin film growth, in many cases by deposition via evaporation of the desired material or by a solution-based process, is typically related to non-equilibrium, i.e. the structure formation is not only determined by the thermodynamic equilibrium of the system and the minimum of the Free Energy, but non-equilibrium statistical mechanics and *kinetics*. We will see that this leads to growth rate equations, and the competition of the time scales of the various processes involved (diffusion, adsorption etc.) will determine the characteristic length scales and morphologies of the forming nanostructures, which, even for seemingly simple film growth, will exhibit laterally nontrivial correlations. This has developed into an independent area of research. We will first discuss simple examples of rate equations and then typical examples of experimental systems and how these can be described by correlation functions. We will try to identify the key observables and how these can be related to the various growth mechanisms.

As the technological foundation for fabricating thin film components, suitable deposition methods are required. The chosen technique needs to be adapted to the respective substrate (lattice matching, thermal expansion, temperature stability, conductivity, etc.). The selection of the technique directly influences the thin film properties. For the preparation of single crystalline thin films e.g., typically epitaxy will be the method of choice. By controlling the growth parameters one can modify the defect structure, surface termination, orientation, grain size, morphology and more. We will therefore introduce an overview over commonly used thin film deposition techniques from the liquid, gas, or plasma phase, including such wide-spread methods as physical and chemical vapour deposition.

If several thin films of different materials are deposited in a vertical sequence, new functionalities can be embedded in the composite structure. Interface control plays a major role in device reliability, and e.g. by band-gap engineering of thin semiconductor stacks, the overall band structure of such heterostructures can be widely tuned.

Moving from two-dimensional extended thin films to further constrictions of the nanostructure geometry, a variety of micro- and nanostructuring techniques has been developed that enable flexible control over the size and shape of nanostructures down to

single nanometers, or even single atoms. We will introduce important top-down and bottom-up methods that are widely used for creating nanostructures by either shaping an existing material into smaller elements, or building up nanostructures from even smaller atomic or molecular building blocks. Lithographic techniques such as photo and electron-beam lithography, several etching techniques, as well as self-assembly strategies will be illustrated with their underlying physical concepts, resolution, examples of typical resulting nanostructures, and application areas.

6.1 Thin film growth: Concepts and theory

Sources:

- T. Michely and J. Krug, Islands, Mounds, and Atoms: Patterns and Processes in Crystal Growth Far from Equilibrium (Springer 2004)*
A. Pimpinelli and J. Villain, Physics of Crystal Growth (Cambridge University Press 1999)
J. A. Venables, Introduction to Surface and Thin Film Processes (Cambridge University Press 2000)
J. Krug, Adv. Phys. 46, 139 (1997), 'Four lectures on the physics of crystal growth'
H. Lüth, Surfaces and Interfaces of Solids (Springer 1993)

6.1.1 Three categories

We consider the adsorption of some film material on a solid substrate.

Generally, three categories of growth scenarios are distinguished (Bauer 1958), which at first glance resemble the situation for wetting and spreading:

- **Frank-van-der-Merwe (FM) growth (layer-by-layer):**
corresponding to complete wetting
- **Stranski-Krastanov (SK) growth (layer-by-layer followed by islanding):**
corresponding to the intermediate case of the 'spreading scenarios' (see Sec.3.6)
- **Vollmer-Weber (VW) growth (islanding):**
corresponding to dewetting (finite wetting angle)

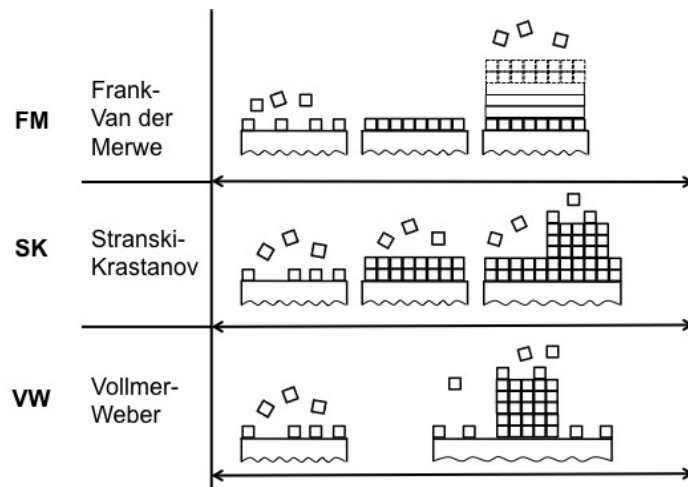


Fig. 6.1: Schematic presentation of the three growth scenarios

The specific conditions, under which these growth modes occur, can be related to the surface or interface tension γ , i.e. the characteristic free energy (per unit area) to create an additional surface or interface.

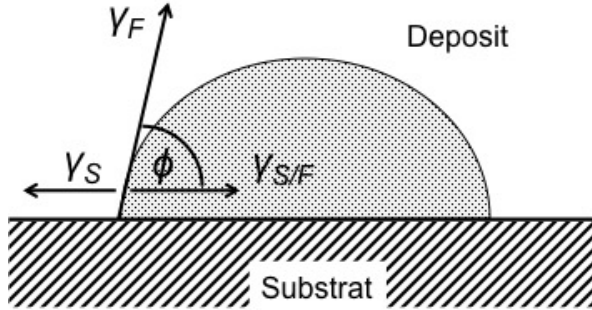


Fig. 6.2: Island on a substrate. Denoted are the different contributions to the surface tension and the contact angle ϕ .

Since γ can also be interpreted as a force per unit length of boundary, force equilibrium at a point where substrate and 3D island of the deposited film touch requires

$$\gamma_S = \gamma_{S/F} + \gamma_F \cdot \cos \Phi \quad (6.1)$$

where γ_S is the surface tension of the substrate/vacuum interface, γ_F that of the film/vacuum, and $\gamma_{S/F}$ that of the substrate/film interface. Using this equation the two limiting growth modes (layer-by-layer, FM) and (islanding, VW), can be distinguished by the wetting angle ϕ .

- FM: $\phi = 0, \gamma_S \geq \gamma_F + \gamma_{S/F}$
- FM: $\phi > 0, \gamma_S < \gamma_F + \gamma_{S/F}$

The mixed mode (SK) can easily be explained in this picture by assuming that there is a lattice mismatch between the deposited film and the substrate. The lattice of the film tries to adjust to the substrate, but at the expense of elastic deformation energy. The transition from layer to island growth occurs when the spatial extent of the elastic strain field exceeds the range of the adhesion forces within the deposited material.

Importantly, however, these considerations are only a 'kinetic analogon' to the wetting scenarios; in fact, since growth is a non-equilibrium process, the surface energies and wetting scenarios can only serve as a limiting case for comparison, but they cannot suffice to properly describe the growth.

6.1.2 How to describe growth?

As pointed out above, surface energies enter the 'equilibrium structure', but actually growth is a non-equilibrium situation, a dynamical problem.

Therefore, dynamical parameters have to enter,

→ the time scale of incoming atoms or molecules (the flux F , which equals the growth rate on the surface only if all incoming molecules are adsorbed and if there is no re-desorption)

→ the time scale of dynamics on the growing surface (i.e. diffusion D), which 'competes' with the time scale set by the flux, so that we can expect that in certain situations the ratio (F/D) is relevant

This already suggests that time dependent equations such as, e.g., rate equations with different kinetic processes are a possible approach to describe growth.

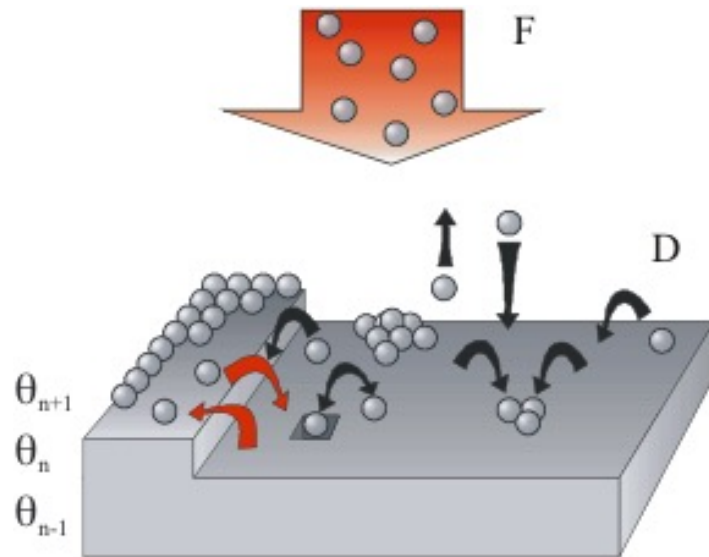


Fig. 6.3: Schematic diagram of processes at a multi-layered surface, including flux F and diffusion D

Of course, the situation is more complex than suggested by only two parameters (or even only one, if exclusively the ratio (F/D) was relevant). In fact, there are several processes contributing to the dynamics on the (growing) surface, and realistically they cannot all be captured in one parameter D.

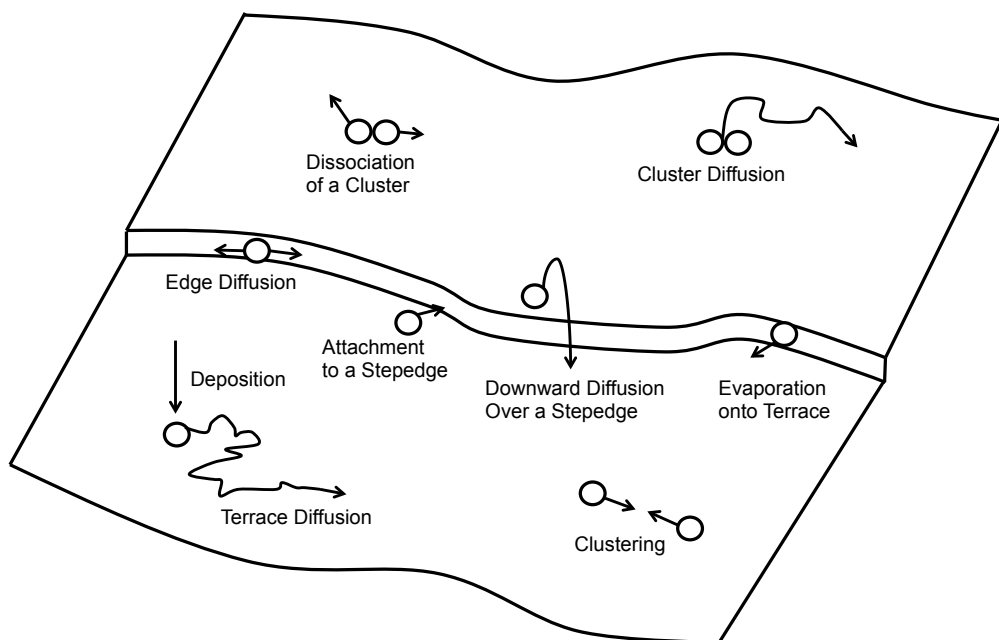


Fig. 6.4: Overview of different dynamic processes occurring in a growing surface

For a system with well-defined layers (e.g., a crystalline adsorbate), the diffusion within one layer (intralayer diffusion) has to be distinguished from the diffusion between different layers (interlayer diffusion). Also, nucleation processes of islands are important. Generally, of course, all these parameters depend on the temperature T. Overall, growth is a rich and still expanding area of science, involving rather advanced (non-equilibrium) statistical mechanics. Here we shall indicate only some basic concepts.

Note that we shall ignore in the following issues such as a possible lattice misfit between substrate and adsorbate for epitaxial systems, although the resulting elastic stress / strain can of course be very important.

Note also that the kinetic description of growth is also relevant for the case that the adsorbate and the substrate are of the same material (which for (single-)crystalline materials would be called homoepitaxy). While in equilibrium we would naively expect the surface of this system to be simply flat, due to the kinetic (non-equilibrium) nature of growth it will not. See, for example, the following pictures of Pt islands grown on a Pt(111) surface. In fact although seemingly not very exciting, homoepitaxial systems as these have been used as very useful model systems for understanding growth.

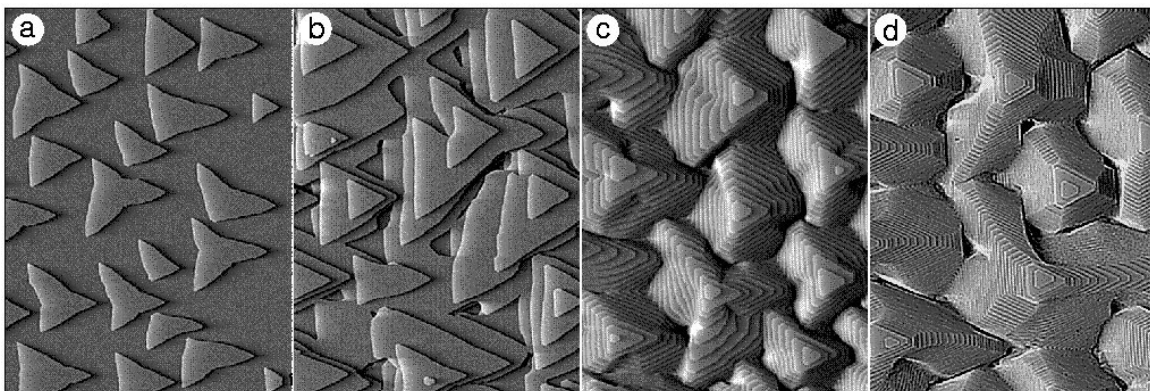


Fig. 6.5: Growth of Pt islands on Pt(111) substrate

In order to get a first idea of the concepts involved, we will discuss two simple growth models. After that, we shall discuss possible refinements of these and other approaches.

6.1.2.1 Intralayer and interlayer diffusion and the Ehrlich-Schwoebel barrier

Generally, of course, there will be some form of transport (diffusion) of the adsorbates. We distinguish

- intralayer diffusion D (diffusion within one given layer)
and
- interlayer diffusion D' (diffusion between different layers)

Intralayer diffusion D (in combination with the incoming flux F) determines to a large extent the typical island sizes and distances in the plane. We will come back to this in

the sections on nucleation and on island sizes and shapes. D will typically depend on the temperature via

$$D = D_0 \exp(-E_D/k_B T) \quad (6.2)$$

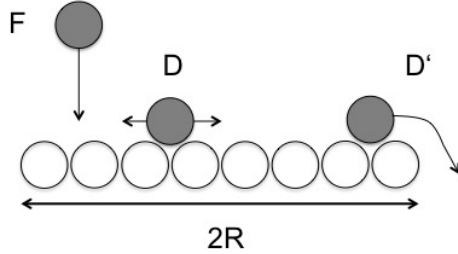


Fig. 6.6: Schematic diagram of intra-layer diffusion \mathbf{D} and inter-layer diffusion \mathbf{D}'

Interlayer diffusion D' usually encounters an additional energy barrier ΔE_S which adsorbates have to overcome for diffusing over an edge into the next layer as shown schematically in Figure 6.7.

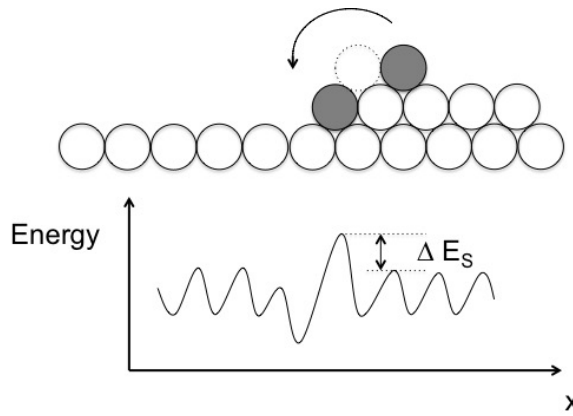


Fig. 6.7: Schematic illustration of surface potential with Ehrlich-Schwoebel barrier at the step edge

This barrier ΔE_S is known as Ehrlich-Schwoebel barrier and usually leads to $D' < D$, i.e.

$$\frac{D'}{D} = \exp(-\Delta E_S/k_B T) < 1 \quad (6.3)$$

A typical order of magnitude is, e.g., $\Delta E_S \approx 0.14$ eV for Pt growth on Pt(111).

6.1.3 Simple growth models

6.1.3.1 Langmuir growth for a monolayer

Consider a system, for which the adsorbate grows only in the first monolayer, and further growth (i.e. occupancy of the second layer etc.) is impossible. This approximates

relatively well the situation for some surfactant systems and self-assembled monolayers (SAMs) of the thiol-on-gold type, but it has little to do with, e.g., the evaporation of, say Au on Si.

The following model is useful to get a feeling for the kinetic equations.

In the simplest case we assume that there is no lateral interaction between different sites, so that the occupancy of a given adsorption site (again, all in the first monolayer) has no impact on the adsorption rate in the neighbouring sites. The adsorption sites in the monolayer are thus considered all independent. The rate of chance of the coverage θ (normalised to one) is thus simply proportional to the incoming flux times F , some probability of adsorption Ω (which we combine in a growth rate $(1/\tau)$), and to the fraction $(1-\theta)$ of unoccupied adsorption sites

$$\frac{d}{dt}\theta = \frac{1}{\tau}(1 - \theta) \quad (6.4)$$

This differential equation is easily solved (with the boundary condition that for the starting time the coverage is zero, i.e. $\theta(t = 0) = 0$)

$$\theta(t) = 1 - \exp(-t/\tau) \quad (6.5)$$

A typical example (taken from thiols on gold) is shown in Figure 6.8.

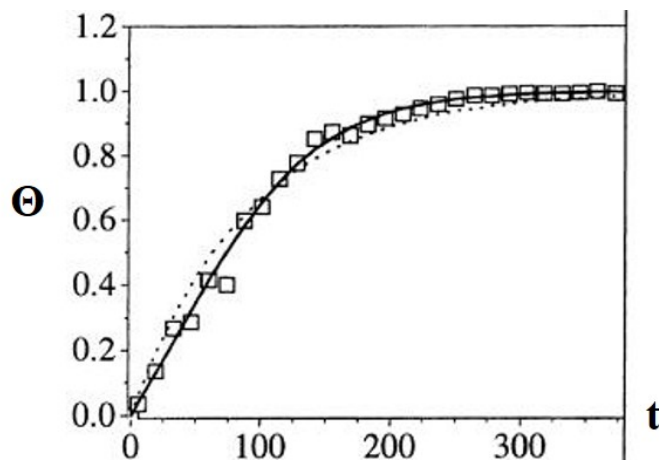


Fig. 6.8: Time dependence of Langmuir growth of thiols on gold

Addendum: Langmuir isotherm (equilibrium monolayer adsorption)

see Desjonquieres / Spanjaard book on *Concepts in Surface Physics*, Springer

While in general thin film growth is an inherently non-equilibrium phenomenon, we consider *as a reference* the adsorption of atoms or molecules from the gas phase on a solid substrate in equilibrium. We will assume for the simplest case that there is a certain binding energy $-E_2$ for the gas phase species on the solid surface, which favors adsorption. We will consider only the first monolayer. We will also assume that this energy is independent of the occupancy of the neighboring sites, i.e. no lateral interactions, and thus no dependence on the total (normalized) coverage Θ .

In equilibrium we will then expect that the rates of desorption and adsorption are equal, i.e.

$$p_2(1 - \Theta) = p_0\Theta \quad (6.6)$$

where the (at this stage unspecified) proportionality constant p_0 is expected to depend on E_2 and temperature T .

Re-arranging this equation gives the equilibrium adsorption at a certain T , i.e. the Langmuir adsorption isotherm,

$$\Theta = \frac{p_2}{p_2 + p_0}. \quad (6.7)$$

The behavior is exactly as intuitively expected, i.e. for low pressures Θ increases linearly with p_2 , whereas for high pressures Θ asymptotically approaches 1. p_0 turns out to be the pressure at which $\Theta = 0.5$.

A more elaborate calculation will specify the dependence on E_2 and T . For this, we involve statistical mechanics and start with the partition function

$$Z(N_{2s}) = C_N^{N_{2s}} \exp \left[\frac{N_{2s} E_2}{k_B T} \right], \quad (6.8)$$

where N_{2s} is the number of adsorbed species and the $C_N^{N_{2s}}$ are binomial coefficients.

The grand canonical partition function can then be written as

$$\Xi = \sum_{N_{2s}=0}^N Z(N_{2s}) \exp \left[\frac{N_{2s} \mu_2}{k_B T} \right] \quad (6.9)$$

After insertion of the expression for $Z(N_{2s})$ we obtain

$$\Xi = \left(1 + \exp \left[\frac{E_2 + \mu_2}{k_B T} \right] \right)^N \quad (6.10)$$

The probability of finding N_{2s} adsorbed atoms or molecules is then

$$P(N_{2s}) = Z(N_{2s}) \exp \left[\frac{N_{2s} \mu_2}{k_B T} \right] / \Xi \quad (6.11)$$

Inserting Ξ we find for the average adsorption

$$\langle N_{2s} \rangle = \sum_{N_{2s}=0}^N N_{2s} P(N_{2s}) = k_B T \frac{\partial}{\partial \mu_2} \ln \Xi \quad (6.12)$$

and thus

$$\langle N_{2s} \rangle = N k_B T \frac{\partial}{\partial \mu_2} \ln \left(1 + \exp \left[\frac{1}{k_B T} (E_2 + \mu_2) \right] \right) \quad (6.13)$$

The normalized coverage is then calculated as

$$\Theta_2 = \frac{\langle N_{2s} \rangle}{N} = \frac{\exp \left[\frac{E_2 + \mu_2}{k_B T} \right]}{1 + \exp \left[\frac{E_2 + \mu_2}{k_B T} \right]} \quad (6.14)$$

This already resembles the result for the Langmuir adsorption isotherm above.

In order to express this as a function of pressure and temperature and not chemical potential, we use the translational partition function of the ideal gas

$$Z_V = \frac{V}{h^3} (2\pi M k_B T)^{\frac{3}{2}} \quad (M: \text{mass}; h: \text{Planck constant}) \quad (6.15)$$

For N_{2s} indistinguishable particles and employing Stirling's formula, we get for the chemical potential

$$\mu_2 = -k_B T \left(\frac{\partial}{\partial N_{2s}} \ln Z_V \right) \quad (6.16)$$

Using the ideal gas law $p_2 V = N k_B T$ to replace V and introduce p_2 , this can be written as

$$\mu_2 = k_B T \ln \left[\frac{p_2}{k_B T} \left(\frac{h^2}{2\pi M k_B T} \right)^{\frac{3}{2}} \right] \quad (6.17)$$

This finally gives the expression for the Langmuir isotherm

$$\Theta = \frac{p_2}{p_2 + p_0}. \quad (6.18)$$

with

$$p_0(T) = \left(\frac{2\pi M k_B T}{h^2} \right)^{3/2} k_B T \exp \left[\frac{-E_2}{k_B T} \right] \quad (6.19)$$

We can also see that, as expected, for strong binding energies E_2 we have a low p_0 , i.e. the adsorption curve tends to 1 already for low p_2 .

6.1.3.2 Multilayer growth without interlayer diffusion ('statistical growth')

We consider a system in which not only a monolayer, but all layers with their respective coverage θ_n can be occupied and grow. As the key ingredient in this model we assume that there is no interlayer diffusion, i.e. a given adsorbate molecule will stay in the layer in which it was initially accommodated and can only diffuse laterally *within* this layer. This model is referred to as 'statistical growth' or also 'random deposition'.

The growth rate of the nth layer is then given by

$$\frac{d}{dt}\theta_n = \Omega F(\theta_{n-1} - \theta_n) \quad (6.20)$$

with the boundary condition $\theta_{n=0} = 1$.

One can show that the solution of this system is

$$\theta_n = 1 - e^{-\theta} \sum_{k=0}^{n-1} \frac{\theta^k}{k!} \quad (6.21)$$

where the total coverage is

$$\theta = \sum_{n=1}^{\infty} \theta_n = \Omega F t \quad \text{with} \quad 0 \leq \theta_n \leq 1 \quad (6.22)$$

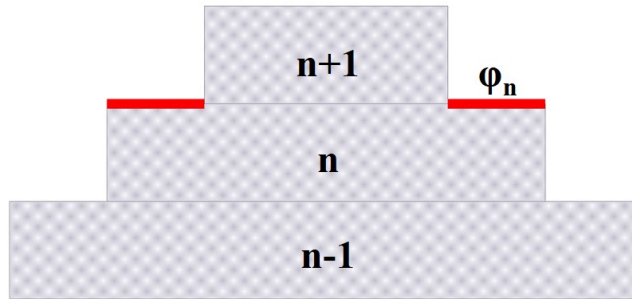


Fig. 6.9: Schematic illustration of the exposed coverage φ_n of the nth layer

The *exposed* layer coverage (i.e., the fraction of a given layer which is *not* covered by the one above it) follows a Poisson distribution

$$\varphi_n = \theta_n - \theta_{n+1} = \frac{e^{-\theta} \theta^n}{n!}, \quad (6.23)$$

which directly follows from (6.21).

This describes the 'terraced structure', i.e. the fractional size of a given layer, the 'envelope' of which has a variance

$$W = \sqrt{\theta} \quad (6.24)$$

characteristic for a Poisson distribution.

The main result is the evolution of the roughness according to

$$\text{roughness} \sim \sqrt{\theta} \quad (6.25)$$

Importantly, the interlayer diffusion does *not* enter this result.

6.1.4 Atomic nucleation theory in 2D

If the nucleus is very small, we can no longer use a continuum picture. We thus employ an atomistic picture.

A simplified approach to dynamical nucleation theory in two dimensions

based on estimates

see Pimpinelli / Villain book see S. Stoyanov / D. Kashchiev in *Current Topics in Materials Science*, vol.7, E. Kaldis (ed.), North Holland, p.69 (1981)

Consider the flux F onto a substrate and the diffusion D in the plane. For simplicity, we set the length scales (typical interatomic or intermolecular distances) to unity, such that F and D have the dimensions of frequency and $1/F$ and $1/D$ have the dimension of time.

Step 1

Estimate the typical nucleation rate of terraces (which eventually reach a size l_s and then coalesce). The terrace reaches a size l_s in a time $O(1/F)$. The average number $l_s^2/(F\tau_{nuc})$ of nucleation events in an area $(l_s)^2$ during a time $1/F$ must be 1.

Thus

$$\frac{1}{\tau_{nuc}} \approx \frac{F}{l_s^2} \quad (6.26)$$

Step 2

Calculate the adatom lifetime τ_1 for diffusion over a length l_s between islands from elementary theory of diffusion

$$\tau_1 \approx \frac{l_s^2}{D} \quad (6.27)$$

Step 3

Calculate (monomeric) adatom density

$$n_1 \approx F\tau_1 \quad (6.28)$$

Combining eq. 3.30 and eq. 3.31 this gives

$$n_1 \approx \frac{F}{D} l_s^2 \quad (6.29)$$

Step 4

Specify critical island size; here we assume that dimers are stable, which is the simplest case. In the literature, this corresponds to $i^* = 1$ (i.e. one adatom is required to make a monomer stable). Then eq. 3.29 gives the dimer nucleation rate $1/\tau_{nuc}$. It is equal to the rate of collisions between adatoms.

Step 5

Estimate the number of sites which an adatom visits in a time $t \dots \approx Dt$. During its lifetime τ_1 the probability of a given adatom hitting an n -atom island is

$$p_n \approx D\tau_1 n_n \quad (6.30)$$

(note that technically there is a correction term $\ln(D\tau_1)$ which we omit, since it introduces only a small modification)

Step 6

The dimer nucleation rate is equal to the rate of collisions between adatoms, i.e. the product of p_1 and F . Combining eq 3.30, eq. 3.32 and eq. 3.33 gives

$$\frac{1}{\tau_{nuc}} \approx F p_1 \quad (6.31)$$

$$\approx FD\tau_1 n_1 \quad (6.32)$$

$$\approx FD \frac{l_s^2}{D} \frac{Fl_s^2}{D} \quad (6.33)$$

$$\approx \frac{F^2 l_s^4}{D} \quad (6.34)$$

and with equation 3.29 we find

$$l_s^6 \approx \frac{D}{F} \quad (6.35)$$

or

$$l_s \approx \left(\frac{D}{F}\right)^{1/6} \quad (6.36)$$

Addendum: Classical (continuum) nucleation theory**a) 3D nucleation**

Nucleation is a classical process for the formation of a new phase. After formation of a nucleus, new material from the environment can diffuse and attach to the nucleus. The key question concerns the stability of the nucleus.

Associated with the formation of a spherical nucleus of a new phase is a change in Free Energy (here in three dimensions).

$$\Delta F = \Delta F_{Volume} + \Delta F_{Surface} = \frac{4\pi}{3}r^3\Delta g_V + 4\pi r^2\gamma \quad (6.37)$$

The interface energy γ of the nucleus is in any event positive. The volume part Δg_V can be negative (i.e. favourable), i.e. $\Delta g_V < 0$. Then the nucleus can be stable above a size r^* . For $r > r^*$ (above the local maximum of ΔF) with

$$r^* = \frac{2\gamma}{\Delta g_V} \quad (6.38)$$

the nucleus is stabilised by further growth (growing r).

b) 2D nucleation

The same picture can be used to discuss the mechanism of the formation of (2D) islands on the surface of a solid. The (possibly stable) nucleus is now two-dimensional, and the boundary (the interface, i.e. the rim) is now one-dimensional. The formation of the interface will also here cost energy ($\sim r$), but this can be (over)compensated by the energy gain proportional to the area of the island ($\sim r^2$), if the island is sufficiently large ($r > r^{**}$).

6.1.5 Island shapes

(see Michely / Krug book, Chapter 3)

The last section was concerned with nucleation, which determines the number density of islands.

This section is concerned with their *shape*. The shape is determined by two additional factors, namely the atomic or molecular processes occurring at the island edge, and the effects of the local environment of the island on the diffusion field of the adatoms. Consider Fig. 6.10 (from Michely/Krug) for an overview of the variety of scenarios of island shapes even for one and the same system (Pt/Pt(111)) when only the temperature is varied, i.e. when different kinetic processes are 'sequentially' switched on.

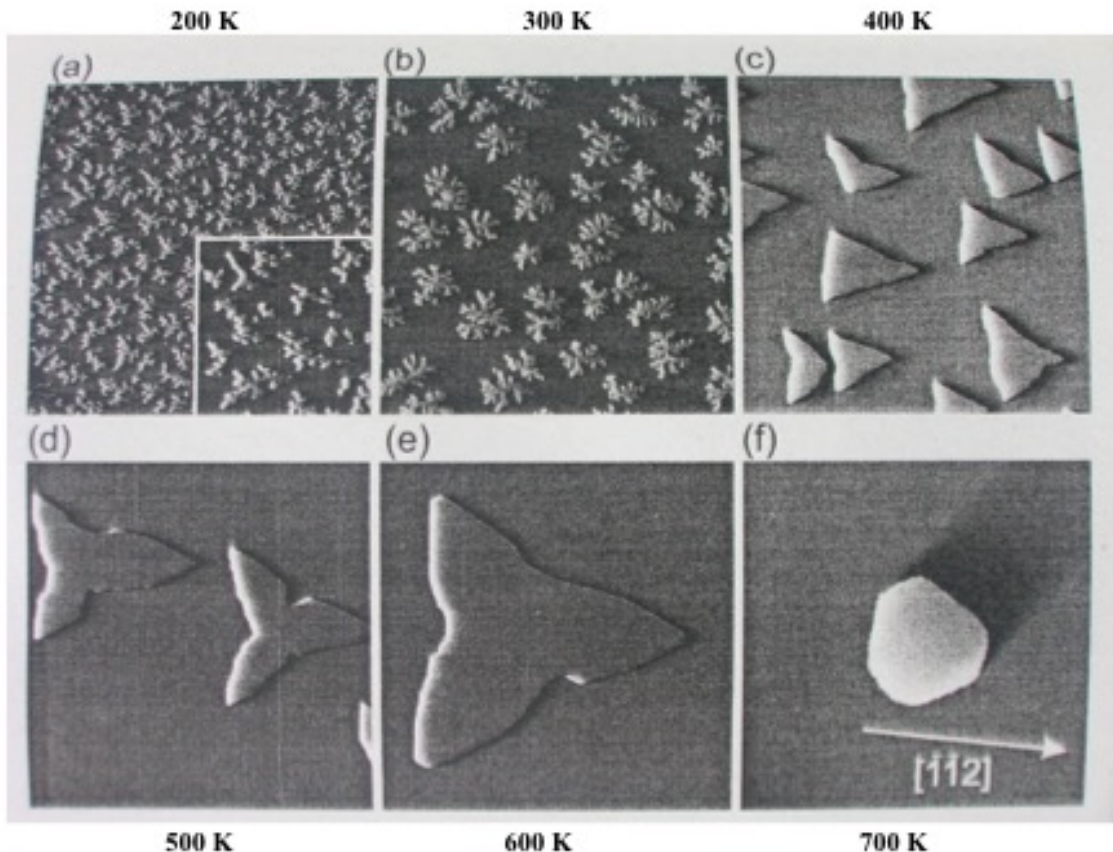


Fig. 6.10: (from Michely/Krug, p.62) Pt/Pt(111) at different deposition temperatures (image size $(156 \text{ nm})^2$), from image (a) to (f) the temperature is increased in 100 K steps. We should learn how to read the shapes ('A snowflake is a letter to us from the sky.' (p.62)).

6.1.5.1 Fractal-dendritic islands

Michely/Krug

(their Sec.3.3, p.81ff; see also Sec.3.6). [http://en.wikipedia.org/wiki/Dendrite_\(crystal\)](http://en.wikipedia.org/wiki/Dendrite_(crystal))

The term 'dendrite' is derived from the Greek word *dendron* ($\delta\varepsilon\nu\delta\rho\nu$) for 'tree'.

This is a rather commonly found morphology for a number of growth phenomena, from snowflakes to islands on metal surfaces and even high-voltage breakdowns (see below).

The formation of fractal-dendritic islands is a common feature in low-temperature homoepitaxial growth on fcc(111) metal surfaces (Michely/Krug, p.81); typically, from the onset of island formation up to $\sim 15\%$ of the melting temperature of the material.

Michely/Krug discuss different types of mechanisms for the formation of fractal-dendritic islands (Sec. 3.3 and Sec. 3.6). We will not go into the details of this rather involved discussion, but refer to the diffusion-limited aggregation model (DLA) below, which helps to rationalize important features of dendrite formation in the limit of low coverage ($\theta \ll 1$) and low island density ($\Omega N \ll 1$), although even in these limits there are important differences to the experiments (Michely/Krug, p.82).

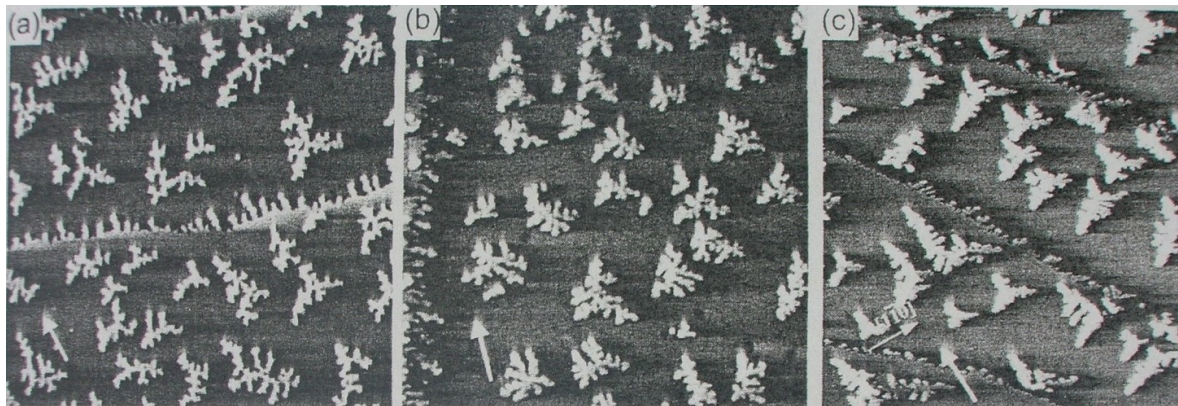


Fig. 6.11: (from Michely/Krug, p.81) Fractal-dendritic islands created by homoepitaxial growth of (a) Pt(111); (b) Al(111); (c) Ag(111), in each case at deposition temperatures around 10 % of T_{melt} . (image size $(120 \text{ nm})^2$).

Diffusion-limited aggregation (DLA) - A simple model

Witten & Sander, PRL 47 (1981) 1400; PRB 27 (1983) 5686 Michely/Krug, p.63; p.81/82; p.100 Wikipedia

A simple model related to, but not identical to dendritic growth discussed above is that of DLA.

A few key points in the context of DLA:

The Eden model is a lattice model, in which particles are added on at a time at random to sites adjacent to occupied sites. This produces relatively compact clusters.

DLA is a variant of the Eden model.

After placing a seed particle at the origin, a second particle is added at some random site at a large distance from the origin. This particle walks randomly (diffuses) until it visits a site adjacent to the seed. There the walking particle then becomes part of the existing cluster. Then the next particle is added, diffuses, and attaches to the existing 'cluster' and so on. The exposed ends of the clusters tend to grow more rapidly than other perimeter sites because perimeter sites near the center are 'shadowed'.

DLA produces aggregates less compact than the Eden model.

The correlation function $C(r) \sim \sum_{r'} \rho(r')\rho(r'+r)$ decays as $C(r) \sim r^{-1/3}$.

The clusters formed in DLA are also referred to as 'Brownian trees'. Of critical importance is that the number of particles undergoing Brownian motion in the system is kept very low so that only the diffusive nature of the system is present.

6.1.5.2 Equilibrium island shapes

(see Michely / Krug book, Chapter 3)

For equilibrium, we expect the island shape to be determined by mechanisms such as the minimization of the surface (i.e. boundary / perimeter) energy. This would correspond to the concept of the Wulff construction. For an isotropic system this

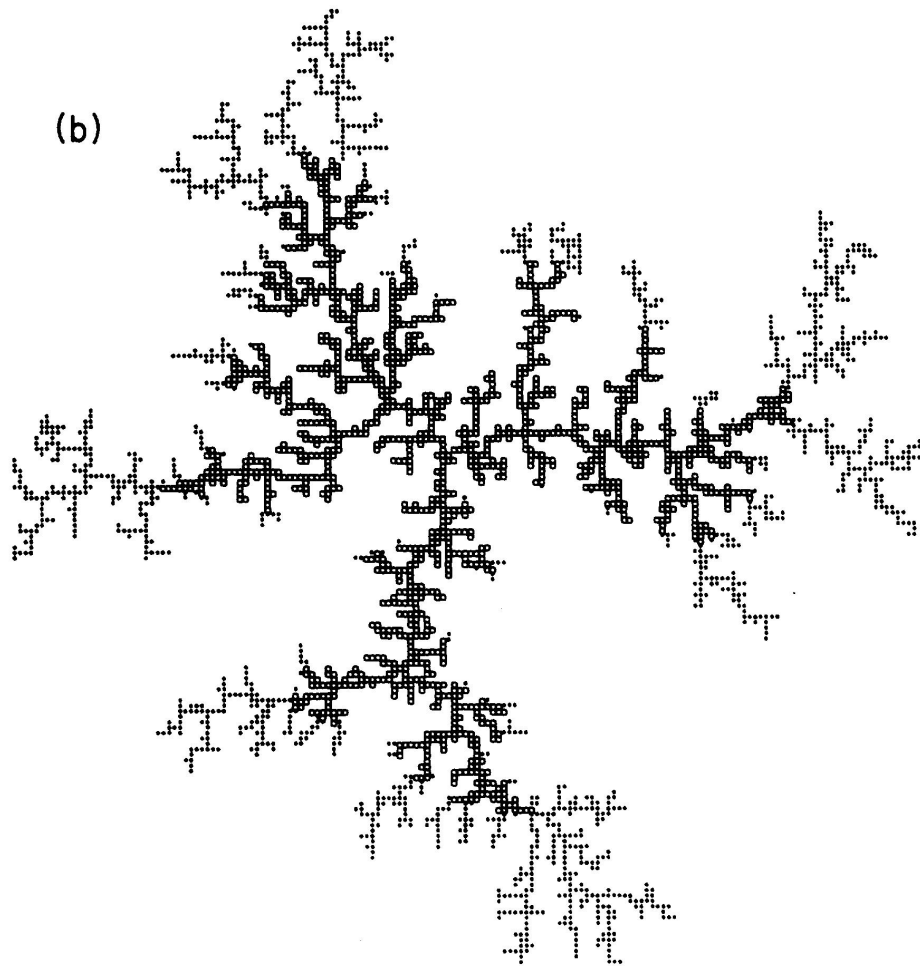


Fig. 6.12: (from Witten & Sander, PRB 27 (1983) 5686) Computer simulation of 3000 particles on a square lattice growing according to DLA. The 'screening effect' is illustrated by showing the first 1500 particles to attach to the aggregate as open circles, the rest (latter 1500 particles) as dots.

would be a circular shape; for a crystalline system, the equilibrium island shape would reflect the crystal symmetry (see Fig. 6.10(f) with the hexagonal island for growth at high temperature, as expected for an fcc(111) surface). Note that for heteroepitaxy (i.e. two different materials on top of each other), strain due to the lattice mismatch will enter the considerations.

If the island shape is *not only* determined by equilibrium energy considerations, but also or even predominantly by kinetic factors, it will be different. This is already demonstrated by Fig. 6.10 (a)-(e), where the island shape obviously deviates from the equilibrium hexagonal (compact) shape.

6.1.6 Epitaxy

The term 'epitaxy' is derived from the Greek *epi* ($\varepsilon\pi\iota$), meaning 'above', and *taxis* ($\tau\alpha\xi\iota\zeta$), meaning 'in ordered manner'. It can be translated as 'arranging upon'. Epitaxy means a defined crystallographic relation between substrate and film, i.e. a defined (relative) orientation of the crystallographic axes. We distinguish

- **homoepitaxy**: substrate and film material are the same ('A on A')
- **heteroepitaxy**: different materials ('B on A')

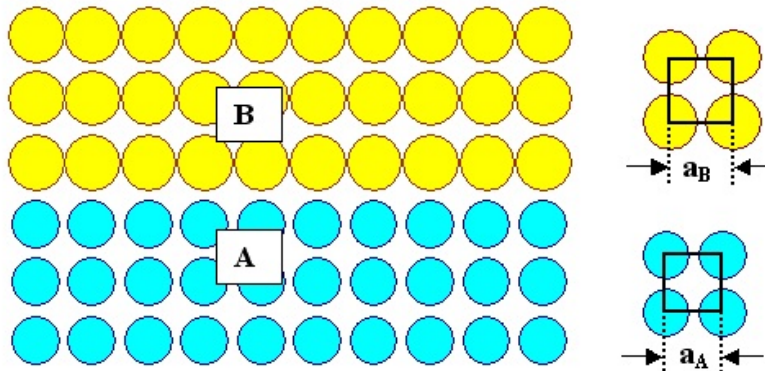


Fig. 6.13: Schematic diagram of heteroepitactic growth of material B on substrate A with identical lattice constants of A and B

Heteroepitaxy will in general lead to epitaxial stress / strain, i.e. a different lattice at / near the interface if the lattice parameters are matched at the interface. A different lattice parameter will in general then lead to different physical properties (i.e. a different gap in a semiconductor, where indeed in many cases 'strain engineering is gap engineering'; see figure 'band gap vs. lattice parameter' below).

Via the epitaxial strain, i.e. the change of the lattice of the film compared to its bulk (intrinsic) structure a new material with new properties can be created. In some cases, the film can even have a completely *different structure*. It is important to realize that a strained lattice costs energy. Calculation of the strain energy (as energy per film volume) can be slightly complicated depending on the specific structure, but typically gives an expression of the type $E \sim Kf^2$, where K is the relevant elastic parameter (bulk modulus ('Kompressionsmodul'); generally anisotropic) and the expression is the typical harmonic approximation (similar to the harmonic oscillator with $E = (1/2)kx^2$ with k = 'spring constant') and the normalized lattice misfit as the key parameter

$$f = (a_{film} - a_{substrate})/a_{substrate} \quad (6.39)$$

In terms of energy per area for a film of thickness d with uniform strain this gives $E \sim Kf^2d$.

Due to this cost in energy the growing film cannot be strained for infinitely large d , since otherwise the strain energy would diverge.

Typical scenarios are:

- 1) Only a very thin film is grown
- 2) After a very thin layer of B on A one continues again with (a thin layer of) A (or some other material with suitable lattice), leading ultimately to a superlattice A/B/A/B/A / ... i.e. (A/B)_n
- 3) If a film (beyond a certain critical thickness) is grown, at some point lattice defects (dislocations) are included to reduce the strain.

The matching of different unit cells at an interface (substrate/film) leads to strain (distortion of unit cell). Note that the structure may also change during growth (structural transition).

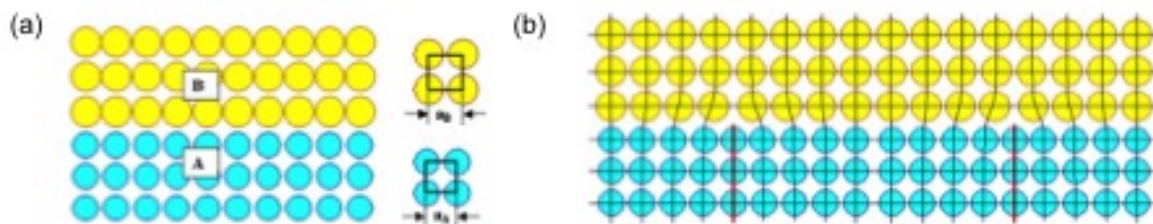
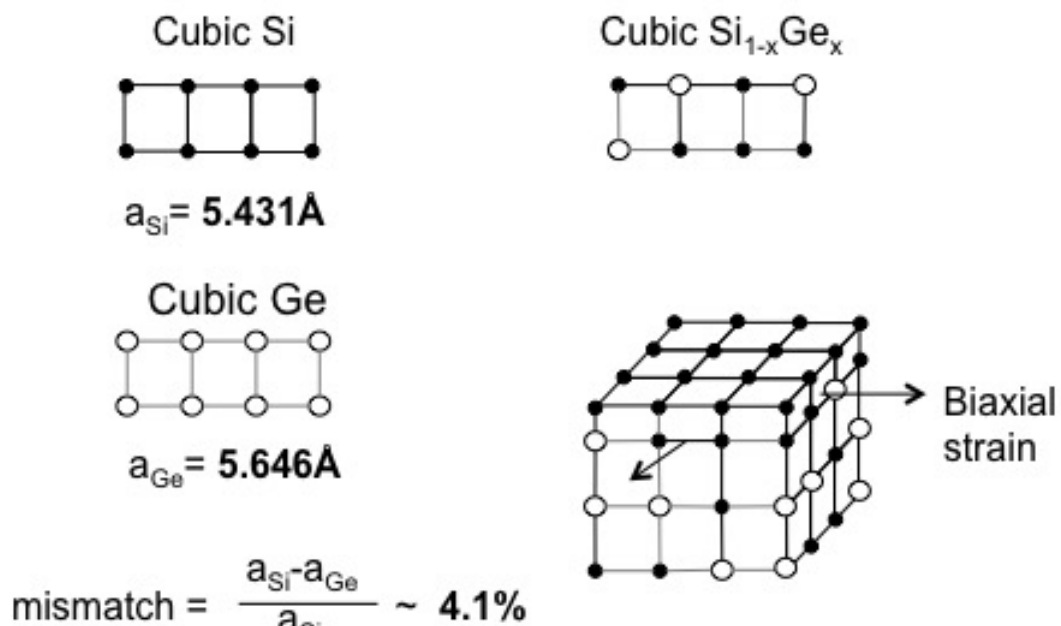


Fig. 6.14: Schematic diagram of heteroepitactic growth of material B on substrate A (a) with identical lattice constants of A and B, (b) with lattice- mismatch, leading to defects and tension at the interface. [http://www.tf.uni- kiel.de/matwis/amat/semitech_en/kap 3/backbone/r3_4_1.html]



○ is Ge atom and • is Si atom

Strained Si on Relaxed $\text{Si}_{1-x}\text{Ge}_x$

Fig. 6.15: Illustration of a typical scenario for lattice mismatch. [http://www.tf.uni- kiel.de/matwis/amat/semitech_en/kap_3/illustr/epitaxy_1.gif]

The calculation for scenario 3) is slightly more ambitious, since it also involves the calculation of the energy associated with a dislocation (see, e.g., Gross/Marx, Festkörperphysik, p. 164 ff.).

Intuitively, it is clear that the result has to be given by the competition of the strain energy and the energetic costs of a dislocation; an approximate result is $d_{critical} \sim b/(10f)$ with the Burgers vector b describing the dislocation (see Weissmantel/Hamann for details).

For a lattice misfit of only 1% the critical thickness is of the order of 10 lattice parameters (i.e. 10 units cells of the film material, i.e about 5 nm).

Thus, already after a rather thin layer there would be many dislocations.

These are typically detrimental for the electronic performance and should be avoided in most cases. This sensitivity to lattice mismatch is a key reason why many potentially attractive combinations of semiconductors are actually not used if smooth films are needed. An example for good lattice matching (low f) is AlAs/GaAs, which both have a lattice parameter of 5.65 Å (while the gap is different (2.16 vs. 1.42 eV), which will be discussed later). An example with bad lattice matching is InAs/GaAs with lattice parameter mismatch 6.06 Å vs. 5.65 Å (f is almost 10 %) so that actually no smooth films, but quantum dots are grown. The gaps are 0.36 vs. 1.42 eV.

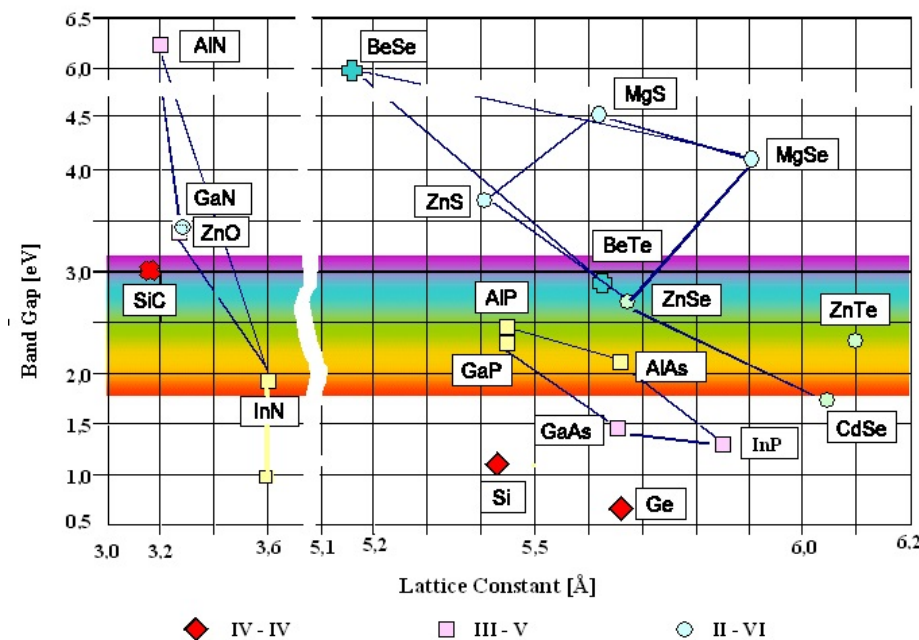


Fig. 6.16: Band gap vs. lattice parameter for various compound semiconductors.
[http://www.tf.uni-kiel.de/matwis/amat/semitech_en/]

A few selected examples

We conclude by showing some examples from the area of semiconductors, but in principle also other materials can exhibit the effects shown here.

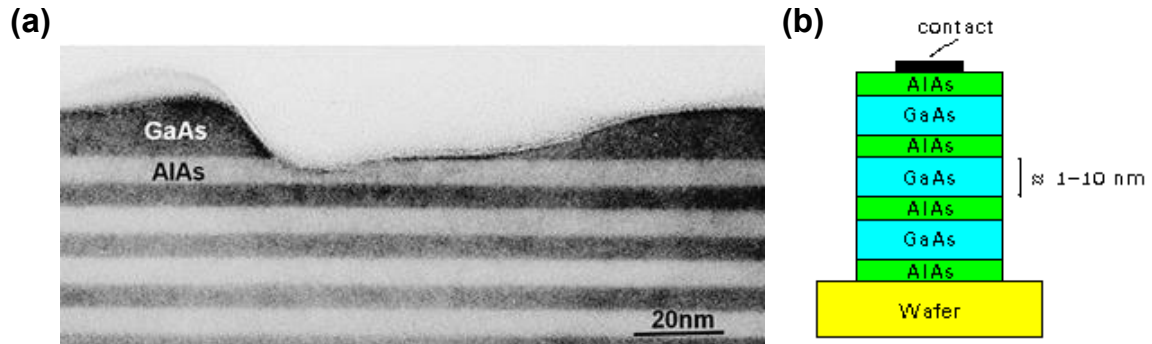


Fig. 6.17: Superlattice (AlAs/GaAs)

See

'structural evolution during formation and filling of self-patterned nanoholes on GaAs (100) surfaces', [Sablon KA, Wang ZM, Salamo GJ, Zhou L, Smith DJ - *Nanoscale Res Lett* (2008)].

Formation of 'quantum dots' by strain-induced 'dewetting'

Note that the strain-induced termination of smooth growth, which may lead to 'dewetting' and thus 'droplets' on the surface may actually be intended for certain applications, such as the controlled growth of quantum dots on surfaces.

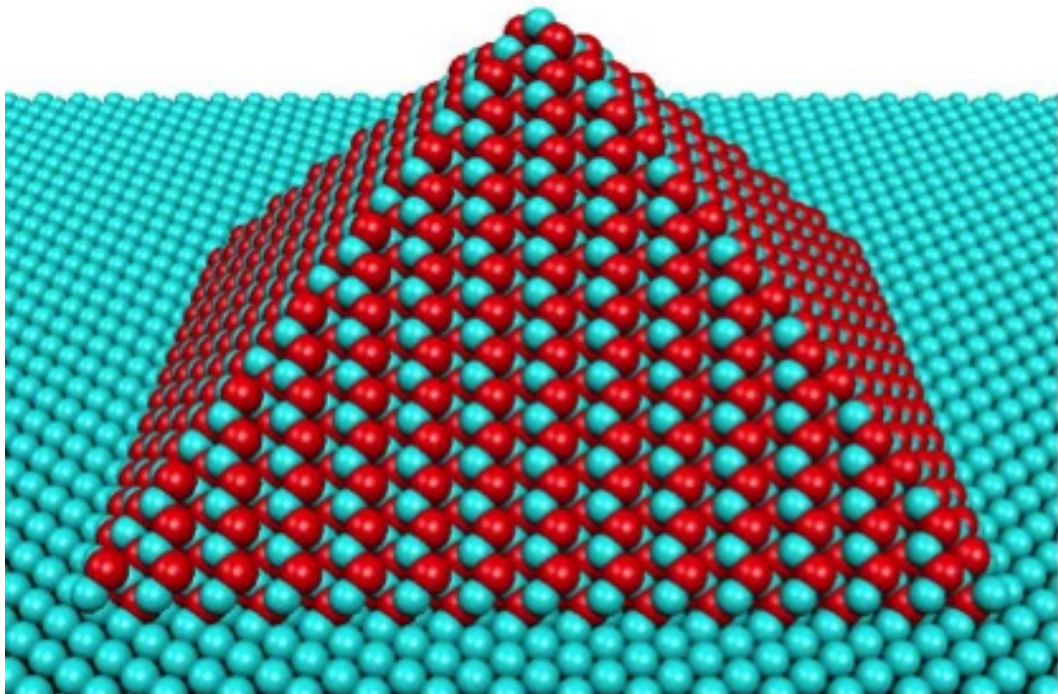


Fig. 6.18: InAs / GaAs quantum dot, see also review 'Spontaneous ordering of nanostructures on crystal surfaces' Shchukin, VA, and Bimberg, D, REVIEWS OF MODERN PHYSICS 71 (1999) 1125. [<http://upload.wikimedia.org/wikipedia/commons/f/f8/QD-pyramide.jpg>]

Si/Ge quantum dot superlattice

Another example is Si/Ge with lattice mismatch 5.65 Å vs 5.43 Å. Quantum dots are grown. The gaps are 0.67 vs. 1.11 eV.

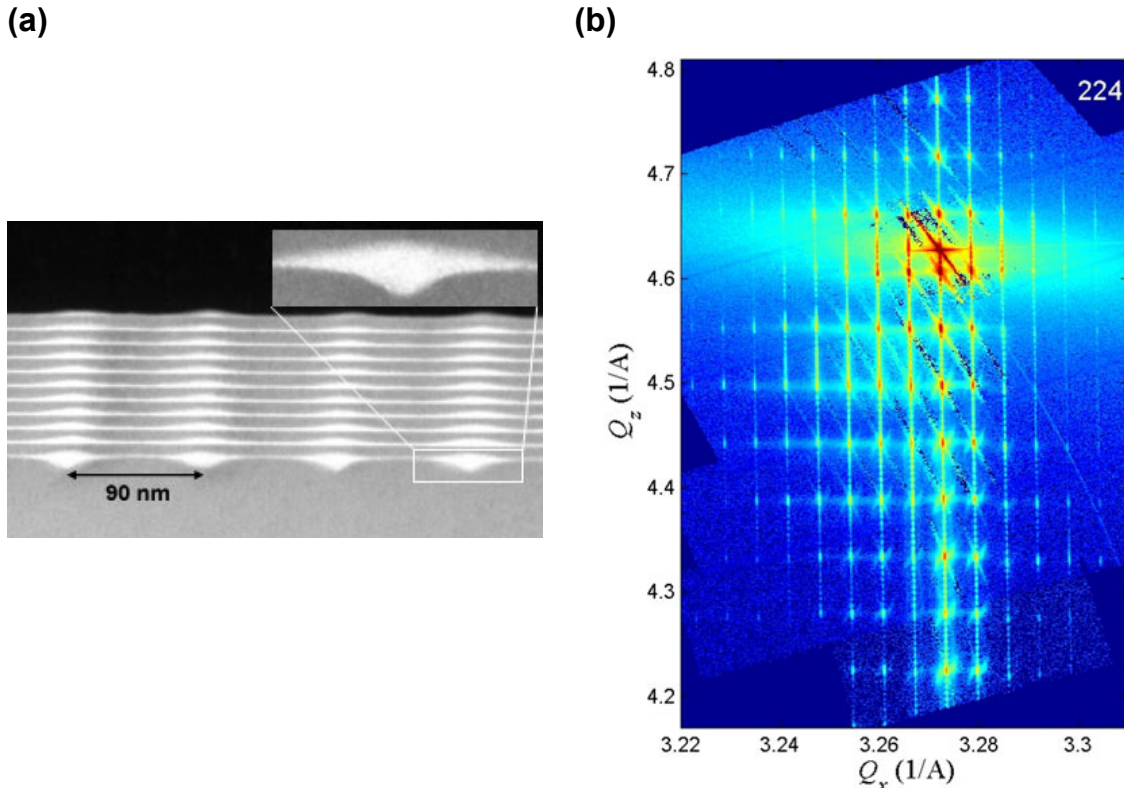


Fig. 6.19: Si/Ge quantum dot superlattice (Ge in Si, i.e. Si spacer layers) with a microscopy image (a) and diffraction (b); see also D. Grützmacher et al., 'Three-Dimensional Si/Ge Quantum Dot Crystals', Nano Letters 7, 3150-3156 (2007). [<http://www.esrf.eu/news/spotlight/spotlight53>]

6.1.7 Some aspects and pictures on growth beyond the monolayer

(see work by Krug and others)

1) Wedding cakes

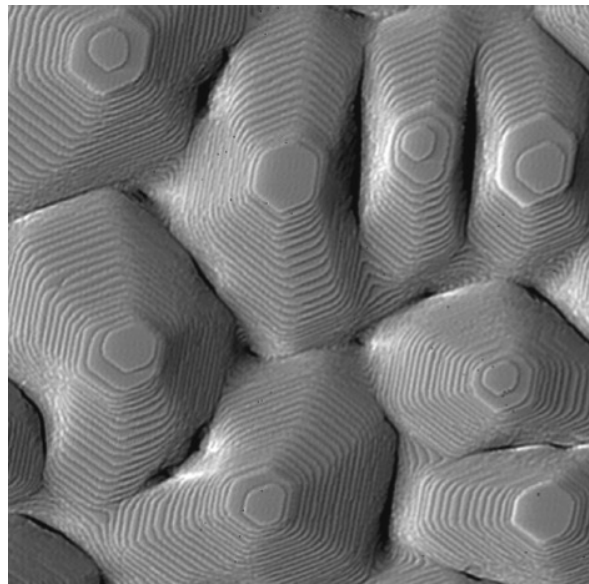


Fig. 6.20: Wedding cakes, (from Krug et al., PRB 61 (2000) 14 037); here Pt/Pt(111) with CO partial pressure.

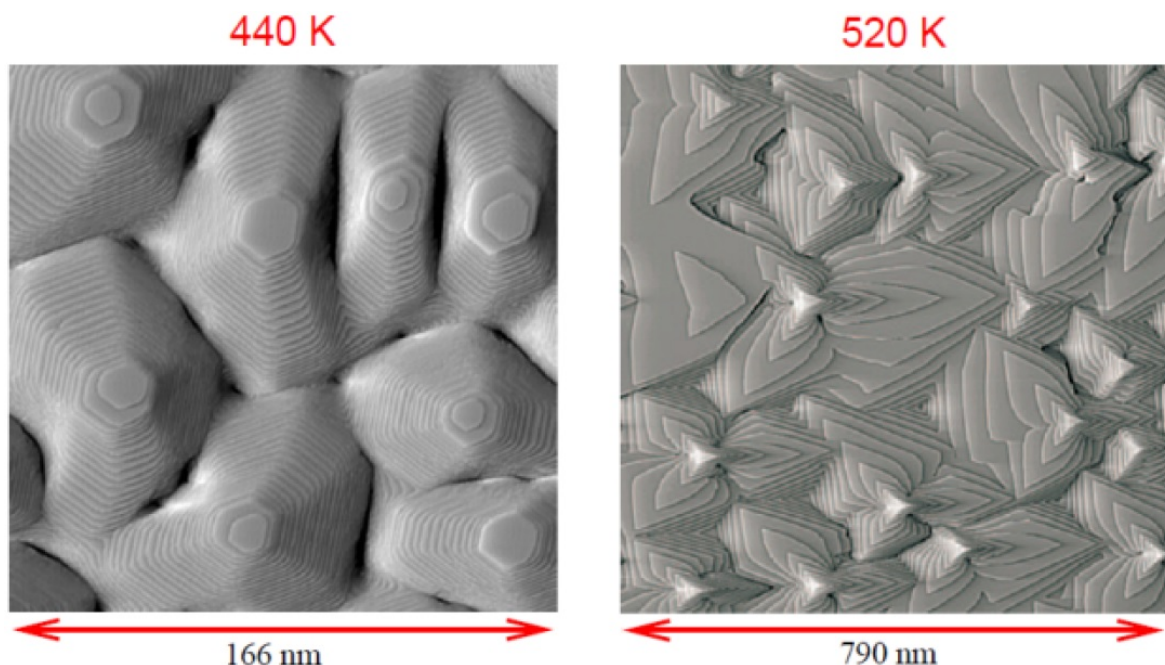


Fig. 6.21: Wedding cakes, (from Krug et al., PRB 61 (2000) 14 037); here Pt/Pt(111) with CO partial pressure.

2) Kinetic growth modes (according to Krug)

(an alternative scheme to FvdM/SK/VW discussed earlier)

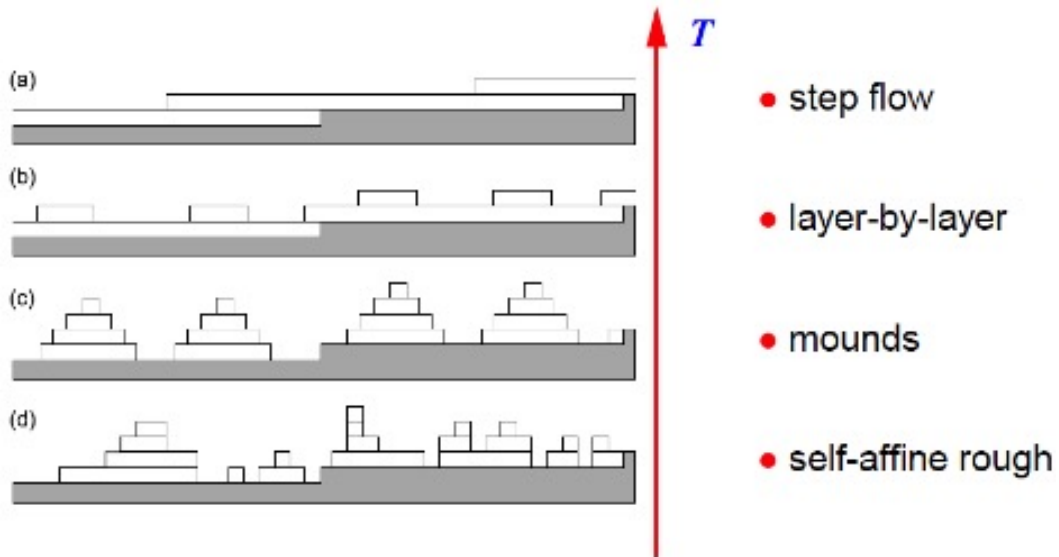


Fig. 6.22: Intra-layer and inter-layer mobility

6.2 Thin film deposition

Thin-film deposition is the deposition of thin layers (films) on a substrate (often single-crystalline) using different techniques.

The various techniques for thin film deposition can be grouped into deposition from a **liquid phase**, from a **gas phase**, and from a **plasma**.

Those methods are often based on **vacuum evaporation processes**: Material is evaporated from one or several sources in high vacuum (HV: $10^{-3} - 10^{-7}$ mbar) or ultra high vacuum (UHV: $10^{-7} - 10^{-12}$ mbar) and then deposited on a substrate.

Important parameters:

- partial pressures p_i (processing gas, residual gas)
- substrate temperature T_s
- deposition rate
- particle energies

Vacuum can be created by using:

- rotary vane/membrane pumps: Compression of residual gas → rough/fine vacuum
- diffusion pumps: Binding of residual gas in oil droplets → HV
- turbo molecular pumps: Removal of residual gas through momentum transfer → HV
- ion (getter) pumps: Ionized particles are removed by electric fields → HV – UHV
- cryo pumps: Freezing of residual particles on cold walls → HV – UHV

The $p_i - T_s$ phase diagram determines the thermodynamic stability of the growing film.

Example: High temperature superconductor $\text{YBa}_2\text{Cu}_3\text{O}_y$ (YBCO):

YBCO is deposited in a tetragonal phase (higher temperature) and subsequently converted into the orthorhombic phase (room temperature, $p_{\text{O}_2} = 1$ bar).

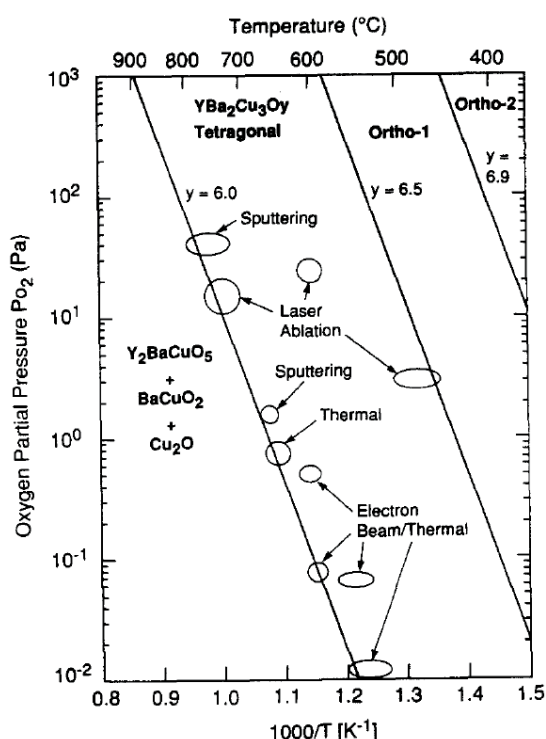


Fig. 6.23: Oxygen partial pressure vs. temperature with critical stability line (left) for $\text{YBa}_2\text{Cu}_3\text{O}_y$ at $y = 6.0$ and parameter ranges for in-situ growth by different thin-film deposition techniques. Also shown is the phase boundary for the tetragonal-to-orthorhombic transition at $y = 6.5$ and the stability line for $y = 6.9$ [R. H. Hammond and R. Bormann, Physica C **162–164**, 703 (1989); Fig.1].

Film growth usually occurs far away from thermodynamic equilibrium

→ Growth kinetics are important and can be very complex, see lecture on film growth.

Depending on the growth conditions, films can be:

- **amorphous** (often requires T_s far below room temperature (RT))
- **polycrystalline** (typical for deposition at RT)
- **textured** (e.g. by directed ion bombardment during growth)
- **single-crystalline** (requires single-crystalline substrates and good lattice match)

Epitaxy (see lecture on film growth) plays a crucial role in the growth of single-crystalline films.

6.2.1 Deposition from the liquid phase

Liquid phase epitaxy (LPE) is an inexpensive technology, suitable for the deposition onto large substrates. It exploits the temperature dependence of the solubility in melts of metal or salt and was used to produce the first useful $\text{Ga}_{1-x}\text{Al}_x\text{As}$ lasers in 1973.

A substrate crystal is brought into contact with a metal melt (e.g. Ga), which is saturated with the material to be grown (e.g. GaAs). When this melt is cooled down, the solubility decreases, and the excess material will grow epitaxially on the substrate.

By combining several metal melts with different growth materials, it is possible to produce complex layer structures.

The *Graphite boat* process (shown in Fig.6.24) leads to relatively high growth rates ($10 \mu\text{m}/\text{min}$).

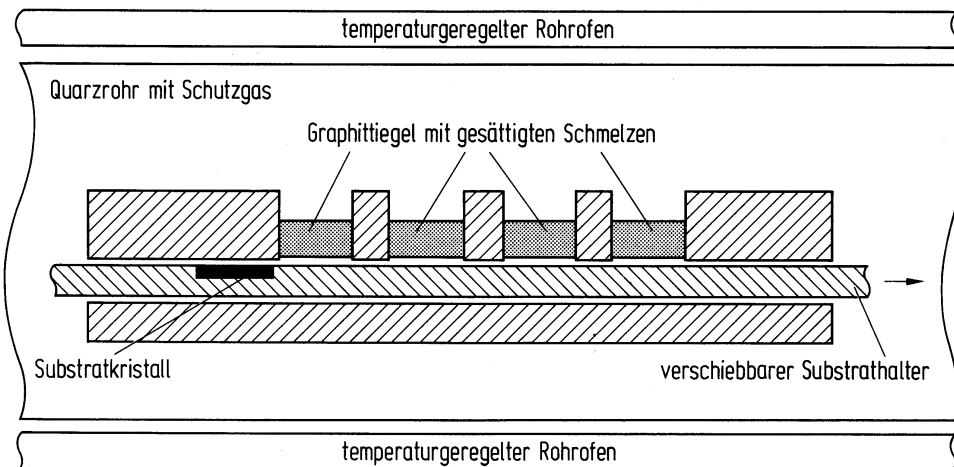


Fig. 6.24: Schematic diagram of a system for liquid phase epitaxy using the graphite boat process [Bergmann-Schäfer, *Lehrbuch der Experimentalphysik*, Bd. 6, Festkörper (1992); Abb.7.37].

6.2.2 Deposition from the gas phase

Material is evaporated from one or several sources in high vacuum (HV) or ultra high vacuum (UHV) and deposited onto a substrate.

- **Thermal evaporation:**

by Joule heating (applying large currents) of a vessel (e.g. molybdenum or tungsten), material in the vessel is melted and then evaporated.

- Low (thermal) energies of particles (0.1 – 0.5 eV):
 $E_{kin} = \frac{1}{2}mv^2 = \frac{k_B T}{2} \approx 100 \text{ meV}$ for $T = 2000 \text{ K}$
- Simple HV process
- Rate control often via resonance frequency shift of piezoelectric quartz crystal due to the deposited mass onto the crystal

- **Electron beam evaporation (EBE):**

Material within a crucible (e.g. Mo, BN, AlO, graphite) is melted and evaporated using an electron beam.

- Rate control via piezoelectric quartz crystal
- Suitable for materials with high melting temperature
- Sequential evaporation using multiple-crucible arrangements

- **Molecular beam epitaxy (MBE):**

Advanced vacuum evaporation process (see schematic diagram in Fig. 6.25)

The individual components of the materials to be deposited are evaporated in *Knudsen cells*:

Heated crucible (temperature T) with small opening (area A_e), vapor pressure $p_e \rightarrow$ evaporation rate $N_e = p_e A_e / \sqrt{2\pi m k_B T}$
 \Rightarrow the material enters the UHV chamber as an atomic or molecular beam and reaches the (usually heated) substrate.

The particle flow rate can be measured by using *mass spectrometry* or *atomic absorption spectroscopy (AAS)*. This allows for accurate control of deposition rates via feedback to Knudsen cells (control of vapor pressure p_e via heating current). Together with the use of fast, controllable shutters for the individual Knudsen cells, one can monitor and control the deposition rates with very high precision.

Often *in-situ* analysis of epitaxial growth (crystal structure and growth rate) is performed by means of electron beam diffraction on the growing surface (*reflective high energy electron diffraction, RHEED*)

\Rightarrow Controlled growth of single-crystalline thin film structures on an atomic level; in particular with a defined sequence of different materials \rightarrow heteroepitaxy.

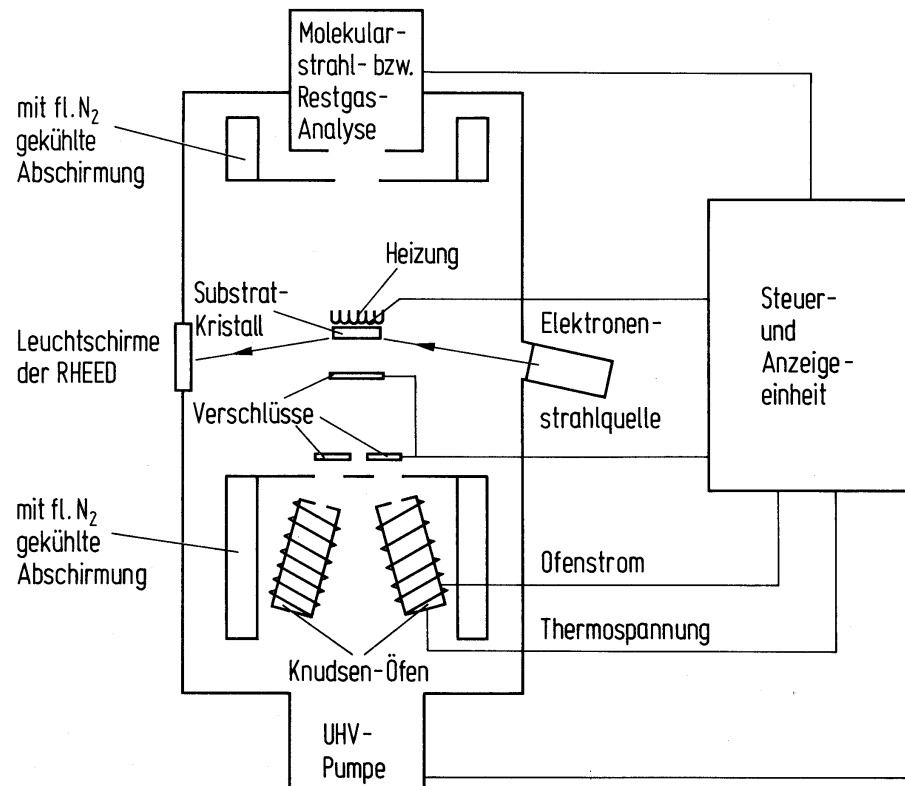


Fig. 6.25: Schematic diagram of an MBE system with analysis of molecular beams and residual gas and in-situ RHEED structural analysis of the growing layers [Bergmann-Schäfer, *Lehrbuch der Experimentalphysik, Bd. 6, Festkörper* (1992); Abb.7.38].

High purity of layers due to process in UHV:

Residual gas pressure $p < 10^{-7}$ Pa = 10^{-9} mbar.

With a sticking coefficient of the residual gas atoms of $H = 1$ and a pressure of $p = 10^{-9}$ mbar, one atomic layer will grow within ~ 20 min.¹

MBE has proved to be highly useful in semiconductor technology for GaAs and corresponding mixed crystals.

More recently, MBE has also been established for the growth of thin films of complex oxide materials ('oxide MBE' for cuprate superconductors, ferromagnetic manganates, and ferroelectric materials (e.g. titanates)), and to combine those materials in advanced epitaxial heterostructures.

Advantages:

- high control over stoichiometric composition
(very flexible, doping can be varied easily)
- in-situ growth control, e.g. via RHEED

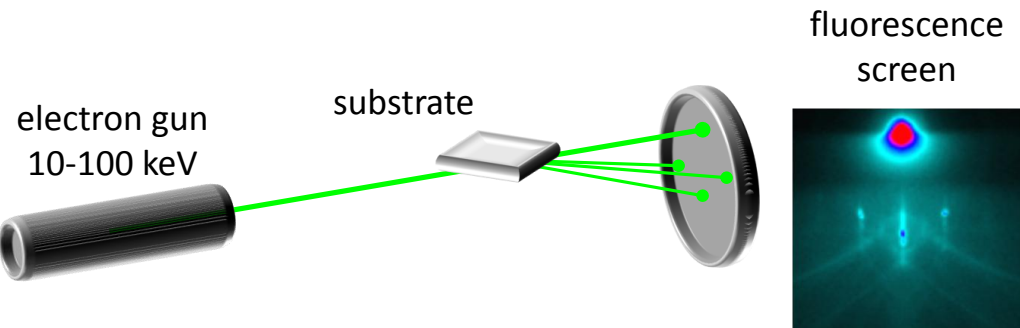
Disadvantages:

- very complex technology → expensive
- even more advanced for growing complex compounds, especially oxides
→ requires use of activated oxygen (e.g. from an ozone source)

¹s. Bergmann-Schäfer, *Lehrbuch der Experimentalphysik, Bd. 5, Vielteilchensysteme* (1992); Abschn. 1.1.1

Addendum: Reflective high energy electron diffraction (RHEED)

Electrons are diffracted on a surface under grazing incidence. The diffraction pattern is visualized on a fluorescence screen (typically recorded by using a CCD camera)



Setup of a RHEED system [J. Tomaschko, Universität Tübingen (2009)]

→ Extremely surface-sensitive method, provides information on crystal structure at the surface (topmost atom layer)

Generation of the diffraction pattern:

The difference between the wave vectors \mathbf{k} (diffracted beam) and \mathbf{k}_0 (incident beam) has to correspond to a reciprocal lattice vector:

$$\mathbf{k} - \mathbf{k}_0 = \mathbf{G}$$

Due to grazing incidence of the electron beam, the lattice is 2-dimensional.

→ reciprocal lattice = infinitely long, parallel lines

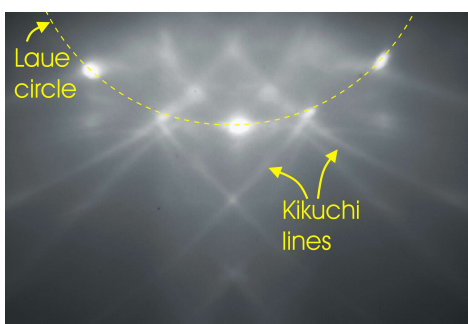
If we consider only elastically scattered electrons, where $|\mathbf{k}| = |\mathbf{k}_0|$, we obtain an Ewald sphere with radius $|\mathbf{k}|$

RHEED reflexes occur at the intersections of the reciprocal lattice with the Ewald sphere!

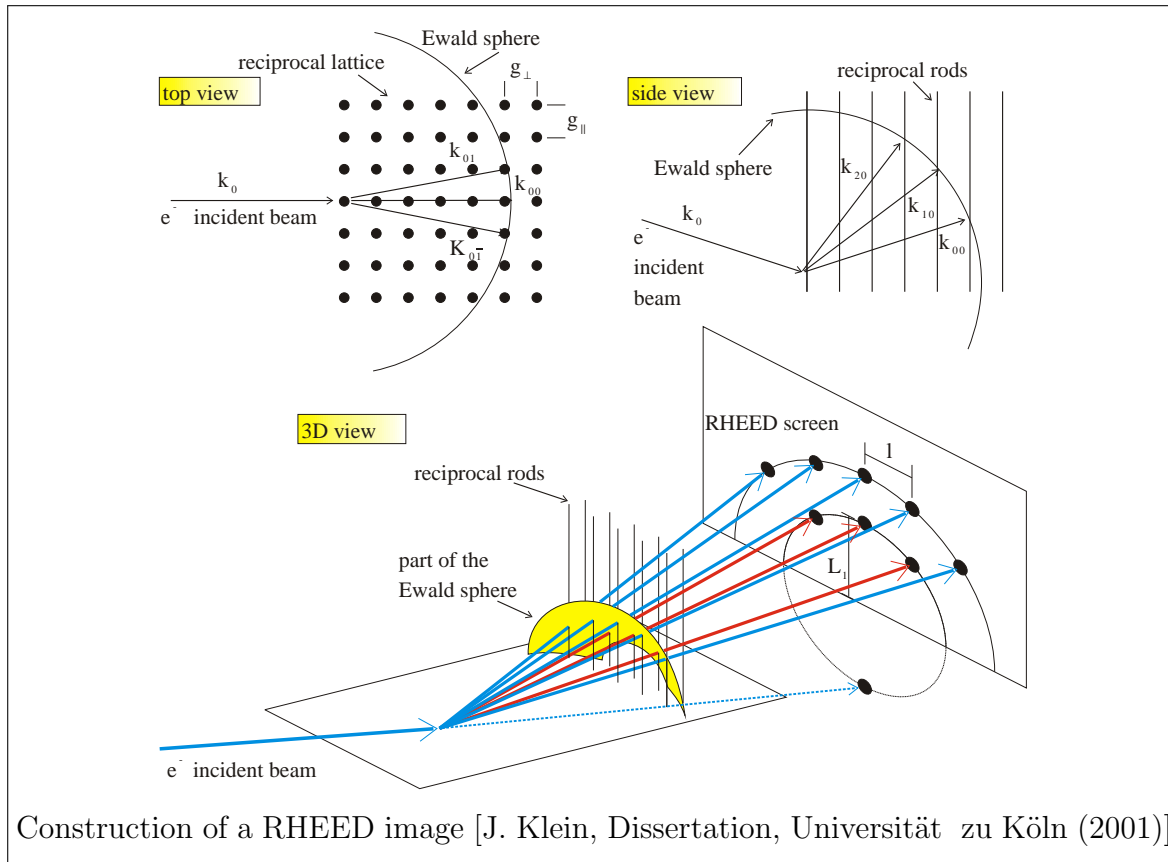
→ reflexes are on 'Laue circles'

Reciprocal lattice vectors can be determined from the position l of the RHEED reflex and the distance L between specimen and screen.

Example:



RHEED image of a SrTiO_3 substrate in UHV. The reflexes are located on the 0th Laue circle. Higher order circles are not shown. The Kikuchi lines occur due to inelastic scattering processes [J. Klein, Dissertation, Universität zu Köln (2001)].



- **Vapor phase epitaxy**
(VPE, or *chemical vapor deposition*, CVD)

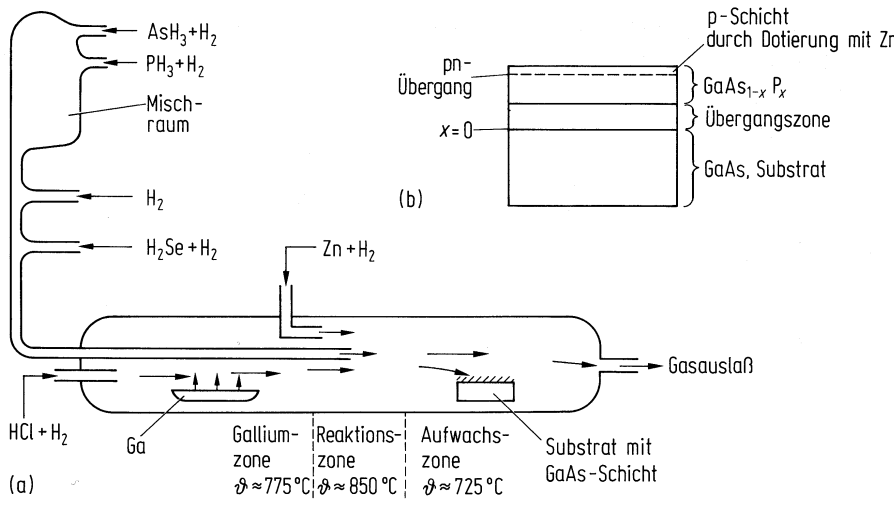


Fig. 6.26:
Fabrication of
 $\text{Ga}(\text{As}_{1-x}\text{P}_x):\text{Se}, \text{Zn}$
light diodes by
vapor phase epitaxy
in a 3-zone fur-
nace [Bergmann-
Schäfer Bd. 6,
Festkörper (1992);
Abb. 7.35].

Vapor phase epitaxy is a technique commonly used in industrial applications. The gaseous components and doping agents are brought together in a reaction chamber, eventually using additional carrier gases. The exact composition and dopant concentration depend on the concentration of the gas mixture \Rightarrow deposition on a substrate (Fig. 6.26). This procedure is also suitable for the growth of carbon materials (carbon nanotubes, graphene).

- **Metal organic chemical vapor deposition (MOCVD, or metal organic vapor phase epitaxy, MOVPE)**

Modern version of CVD – metals are inserted as easily decomposable methyls or ethyls (Fig. 6.27)

Advantages include the ability to precisely control the flow of gases, and a small reaction chamber ⇒ uniform growth with ability to control individual monolayers.

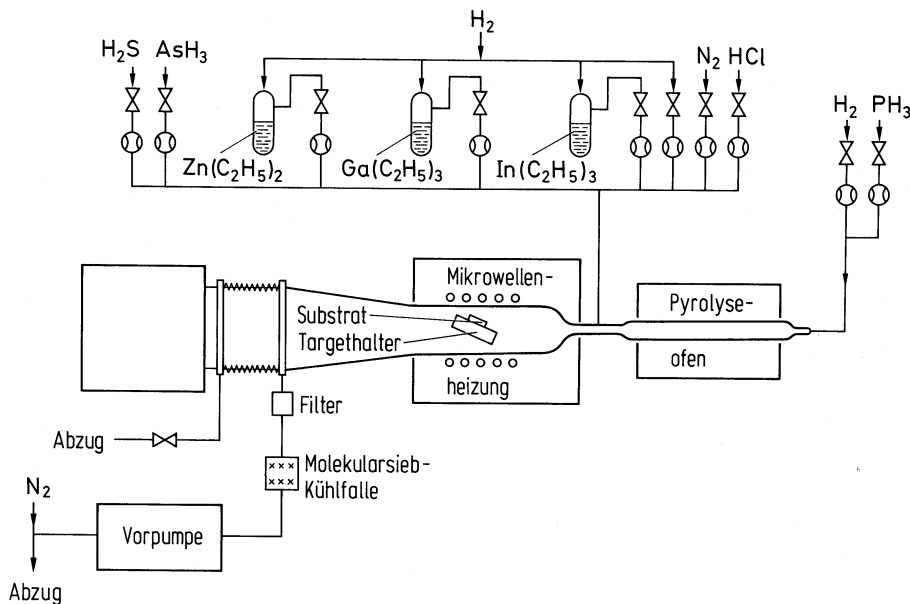


Fig. 6.27: Schematic diagram of an LP-MOCVD system [Bergmann-Schäfer, *Lehrbuch der Experimentalphysik, Bd. 6, Festkörper* (1992); Abb.7.36].

- **Organic molecular beam deposition (OMBD)**

Method to create amorphous and crystalline organic thin-films from small molecules. The molecules are sublimated from evaporator cells in UHV. In contrast to MBE with inorganic semiconductors, a lattice match is not necessary. Growth is usually conducted at substrate temperatures from 77K up to room temperature or at moderately increased temperatures. The evaporation temperatures are relatively low ($\sim 100^{\circ}\text{C} - 450^{\circ}\text{C}$), in order to avoid thermal degradation of the organic precursor materials.

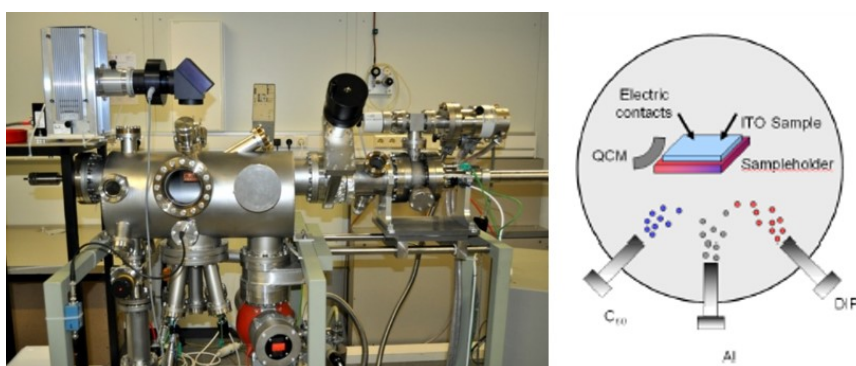


Fig. 6.28: Photograph and schematic diagram of an OMBD system [AG Schreiber, Universität Tübingen].

6.2.3 Deposition from the plasma phase

- **Sputtering:**

vacuum chamber vented with a process gas – typically argon
typical pressures $p = 10^{-3} - 1$ mbar
 \rightarrow mean free paths $\ell = 10$ cm – 0.1 mm

A dc or ac voltage (~ 0.2 – several kV) applied between anode and cathode accelerates free electrons \Rightarrow ionization of Ar atoms $\rightarrow \text{Ar}^+$.

\Rightarrow Ignition of a plasma: The discharge voltage U_D depends on the ‘reduced’ pressure $p \cdot d$ (with d = electrode distance).

$$\rightarrow \text{Paschen's law } U_D = \frac{A \cdot p \cdot d}{\ln(p \cdot d) + B} \quad (A, B: \text{constants, depending on gas type})$$

This yields a minimum in $U_D(pd)$: With increasing pd , the ionization probability is decreased (since $\ell \propto 1/p$; electric field $E \propto 1/d$) \rightarrow kinetic energy of electrons $E_{kin,e}$ too low; decreasing pd leads to too low electron–Ar collision rates

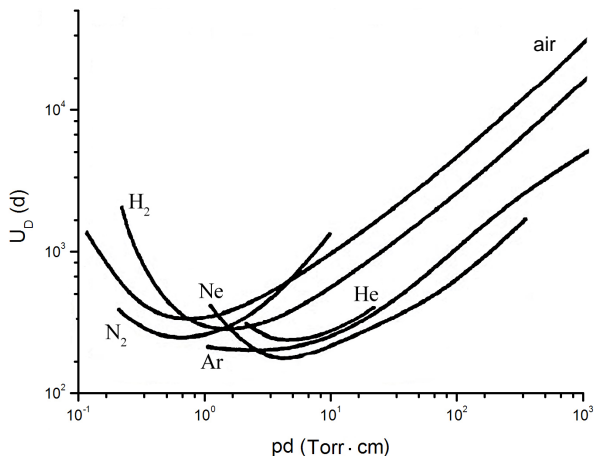


Fig. 6.29: Discharge voltages of different gases, depending on reduced pressure pd (‘Paschen curve’) [Ch. Gürlich, Diploma Thesis, Univ. Tübingen (2005); Fig. 2.9].

Ions are accelerated towards a negatively charged target (mounted on the cathode; contains the material to be deposited) and expel material from the target by momentum transfer. The expelled target atoms then diffuse towards the substrate and grow as a thin film on it.

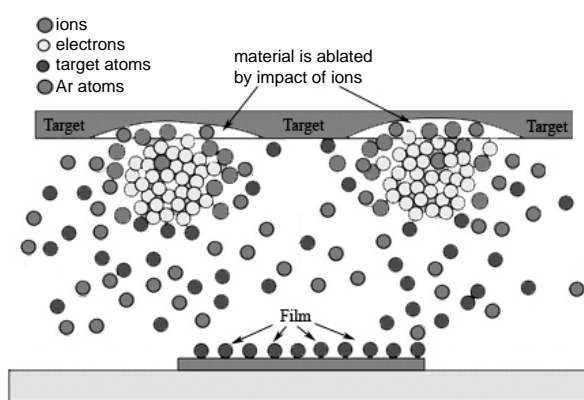


Fig. 6.30: Sketch of the sputtering configuration and process [Ch. Gürlich, Diploma Thesis, Universität Tübingen (2005); Fig. 2.11].

The energy of the atoms arriving at the substrate can be high (1 – 100 eV). This depends on cathode voltage, target-to-substrate distance, and working pressure.

dc sputtering: a dc voltage is applied to the cathode; works with electrically conducting targets.

magnetron sputtering: electron trajectories wind around magnetic field lines
 → reduced ‘effective’ mean free path
 → increased ionization rate (allows lower working pressure)
 → increased sputtering rate → higher energy of target atoms (if p low)

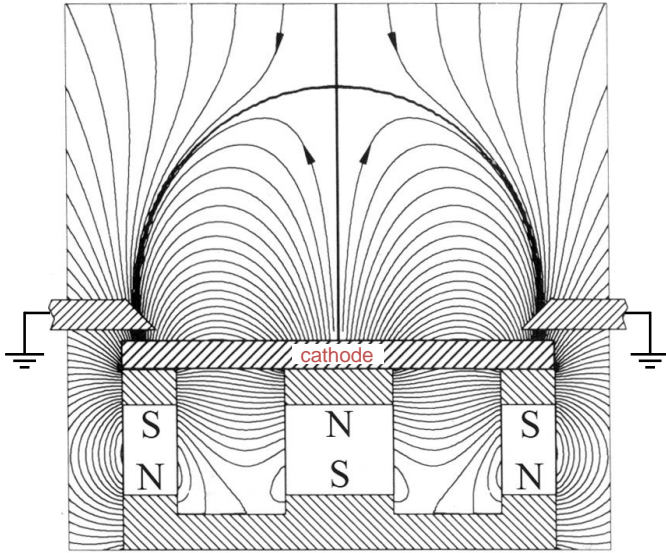


Fig. 6.31: Magnetic field configuration of a rotationally symmetric planar magnetron. Three magnets are attached below the target [Ch. Gürlich, Diploma Thesis, Univ. Tübingen (2005); Fig.2.10].

Radio frequency (rf) sputtering

The application of an rf voltage (~ 10 MHz) allows for sputtering with insulating targets: Since the mobility of electrons in the plasma is significantly higher than that of ions, the target is charged negatively ('self-biasing effect') and is thus bombarded by the (positively charged) ions.

Reactive sputtering:

The inert working gas (Ar) is mixed with a reactive gas (mixture): Usually O₂ or N₂ → growth of oxides or nitrides, e.g. SiO₂, Al₂O₃, Si₃N₄, AlN

Some remarks:

- resputtering:
 acceleration of negatively charged ions (e.g. O²⁻) towards the substrate
 → ablation of the growing film!
 Can be avoided with ‘off-axis’ arrangements or high pressure sputtering (thermalisation of O²⁻ ions before they reach the target)
- Simple HV process (but relatively low growth rates) → industrial use
- suitable for materials which are difficult to (thermally) evaporate
- allows for stoichiometric transfer of complex compounds
 → common method for complex oxides (e.g. cuprate superconductors)
- film growth can be manipulated by adjusting plasma properties (gas composition, voltage)
- In situ rate control difficult
 → determination of rate via film thickness measurements on test samples;
 easily reproducible

- **Pulsed laser deposition (PLD):** A focused, pulsed laser beam (wavelength in the UV range) can ablate atoms from a target surface (direct breaking of chemical bonds – no thermal evaporation)
→ formation of plasma plume – substrate is placed at the tip of the plume

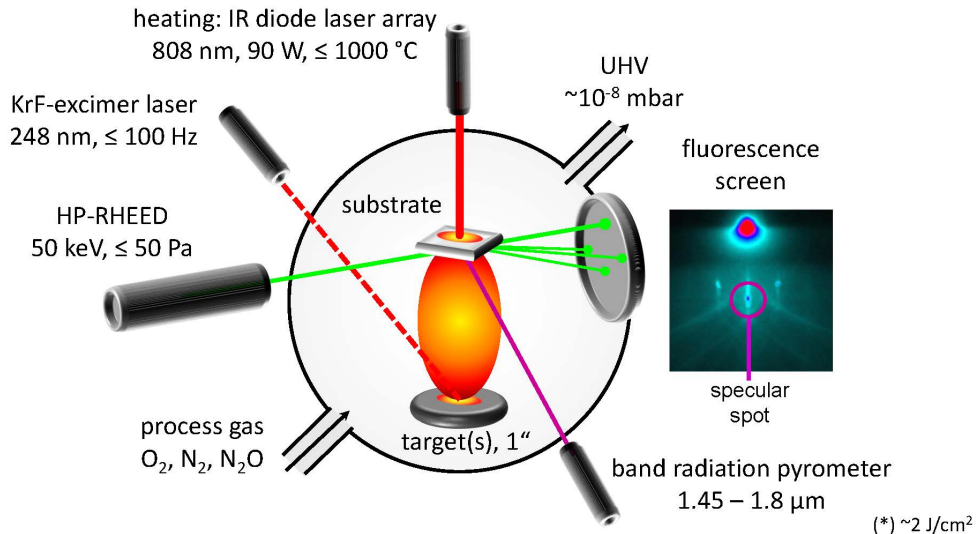


Fig. 6.32: Principle of pulsed laser deposition with in-situ, high-pressure RHEED [J. Tomaschko, Univ. Tübingen (2009)].

- typical laser: KrF-excimer laser ($\lambda = 248$ nm)
- typical pulse lengths: ~ 20 ns
- typical energy densities: ~ 1 J/cm² (can be varied with optics)
- process pressure comparable to sputtering (often O_2 or Ar/ O_2 is used for oxides)

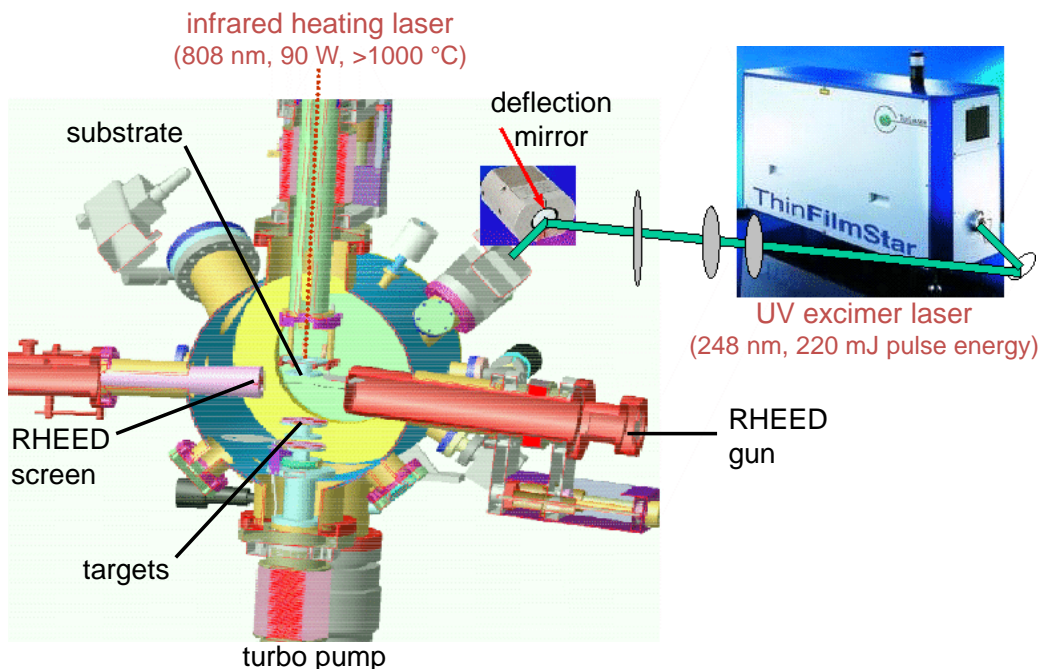


Fig. 6.33: Layout of the PLD system at AG Kühle/Kleiner, Univ. Tübingen [Manufacturer: PINK, Wertheim].

Advantages:

- Relatively easy process for stoichiometric transfer, also for complex compounds;
→ used especially for epitaxial growth of complex transition metal oxides
(cuprate superconductors, mixed valence manganates, titanates etc.)
- No problems with insulators
- Very flexible regarding the choice of material
→ target carousels (~ 4 - 6 targets) ⇒ easy to switch between materials
→ Very well suited for deposition of (heteroepitaxial) multilayers
- In contrast to magnetron sputtering: Possibility to use (high-pressure) RHEED for in-situ growth control (Figs. 6.32, 6.34).
→ Possibility to “count” single monolayers
→ Provides information on relaxation times and the growth mode
(Frank-van der Merwe, Vollmer-Weber etc.)

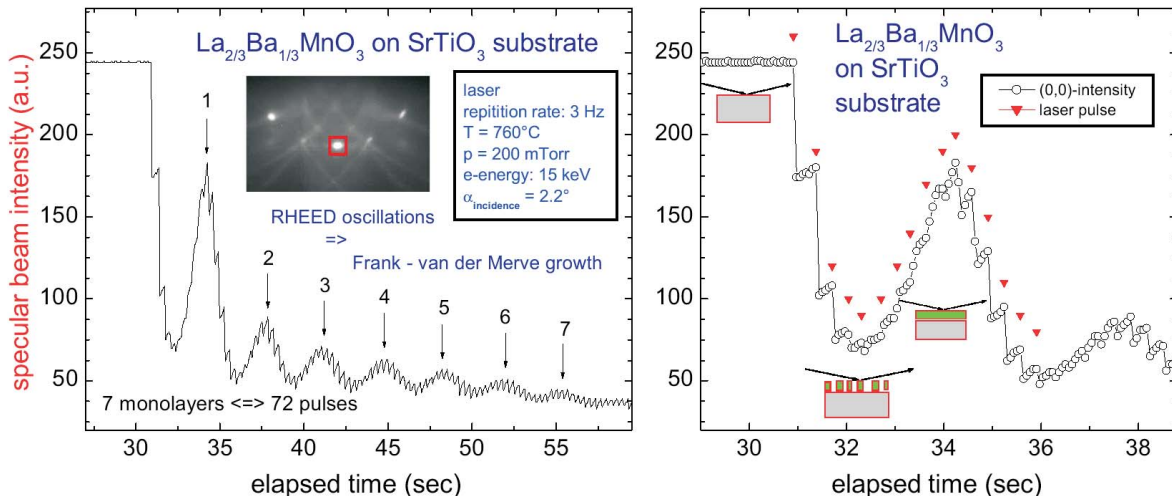


Fig. 6.34: RHEED oscillations during PLD growth of $\text{La}_{2/3}\text{Ba}_{1/3}\text{MnO}_3$. [J. Klein, Ph.D. Thesis, Univ. Köln (2001); Fig. 5.10].

Disadvantages:

- Homogeneous coating of large substrates difficult
(can be remedied by using special geometries/arrangements, is e.g. used for YBCO coating of steel tapes of > 1 km length)
- Optimum growth conditions at the tip of the plasma plume
⇒ optimum substrate-to-target distance depends on many parameters
(Laser energy, energy density, working pressure)
- Requires measures to prevent the formation of precipitates (“droplets”)
(Polishing of target surface, target rotation)

Example: UHV cluster tool:

Combination of different processes in a multi-chamber system

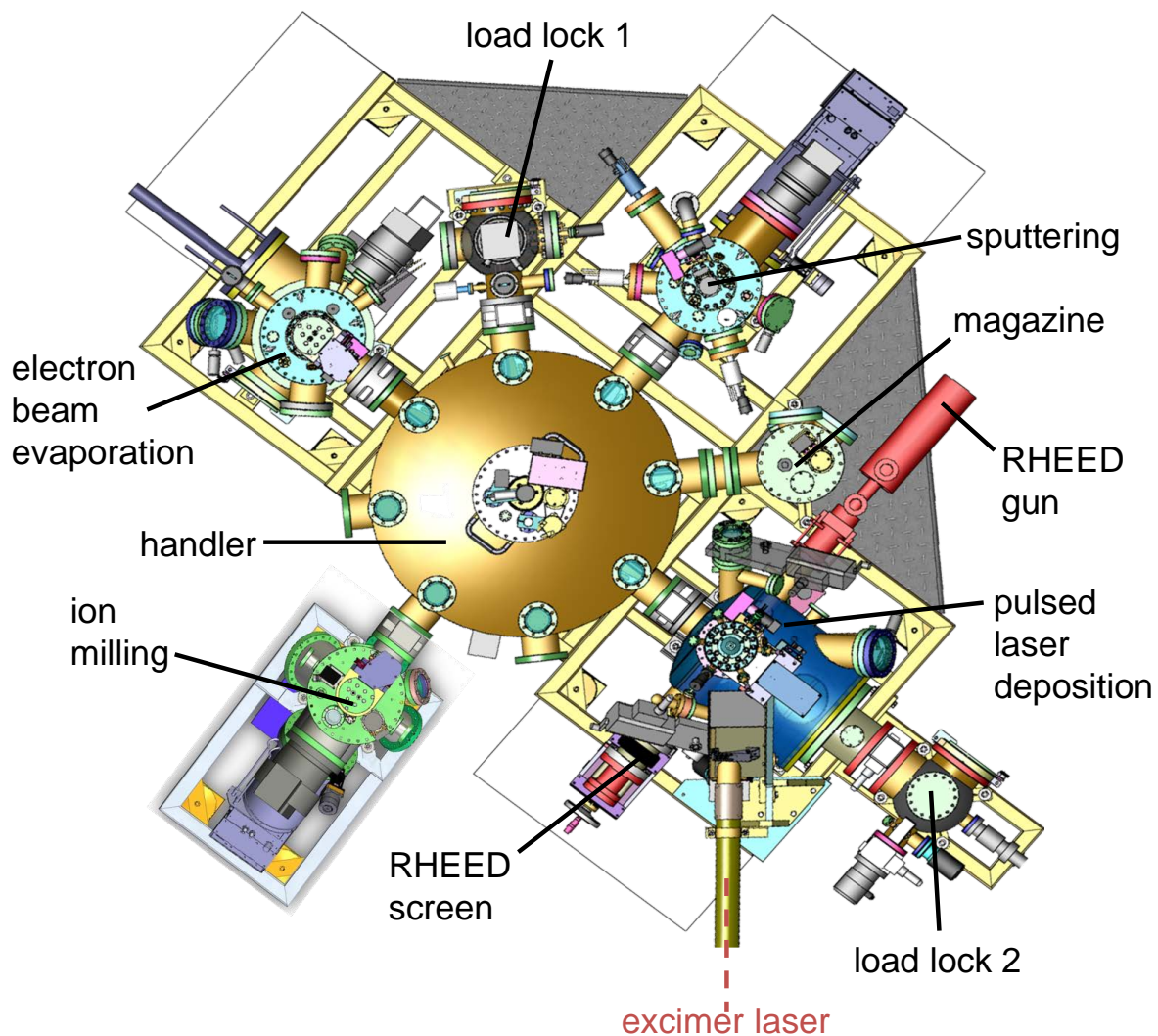


Fig. 6.35: UHV cluster tool [AG Kölle/Kleiner, Univ. Tübingen; Manufacturer: PINK, Wertheim].

UHV system (base pressure $\sim 10^{-9}$ mbar)

Process chambers: e-beam evaporation, sputtering, PLD (with RHEED), ion milling

Sample transfer in UHV via central manipulator (handler chamber)

Sample loading and extraction via load-lock chambers

Sample deposit in magazine chamber

\Rightarrow in-situ combination of different PVD techniques in UHV

\Rightarrow Fabrication of reproducible interfaces

6.3 Micro- & Nanopatterning

The realization of thin film structures for basic research and device applications requires the lateral confinement of the film geometry by suitable micro- or nanopatterning techniques.

There are two basically different approaches for the realization of micro- or nanostructures:

- The **top-down approach** applies nanofabrication techniques (lithography, etching, ...) to a large system (bulk material or a thin film) to “carve out” nanostructures.
 - advantages: flexibility and control regarding shape and position;
 - disadvantage: limited miniaturization ($\sim 5 - 10 \text{ nm}$)
- The **bottom-up approach** starts with small components (atoms, molecules, quantum dots, colloids), which are then assembled to form somewhat larger entities by using nanotechnological or (surface-)chemical methods in order to create a desired nanostructure.
 - advantages: very small structures possible, often self-assembling systems;
 - disadvantages: limited shapes and often lack of control of position

For the realization of lateral structures in thin films within the range of micro- and nanometers, usually a combination of lithography and etching is applied. Recently, direct patterning (removal of material) with a focused ion beam (FIB) has found increasingly widespread use.

6.3.1 Lithography

Lithography is based on the realization of a resist structure in a suitable material (resist), deposited directly on top of a thin film or substrate. The resist can be patterned with photons, electrons, ions, stamps, Subsequently, the pattern is transferred by various possible processes (deposition, etching, doping, ..., see Secs. 6.3.2, 6.3.3).

Lithography processes are usually done in a **clean room** under controlled environmental conditions (temperature, humidity) with reduced (often as low as possible) concentration of dust particles. In case of light-sensitive resists one has to work in a room with yellow light, in which the high-energy spectrum of the visible light sources is filtered.

Usually, the liquid **resist** (a polymer in some solvent) is deposited by **spin coating**, i.e. by placing a drop of resist on a centrifuge ('spinner') with high revolution speed (few 1000 rpm). Typical resist thicknesses are several 100 nm up to a few μm . Alternatively, one can apply **dip coating** (substrate is dipped into resist and pulled out slowly), or **spray coating** (resist is sprayed onto the substrate; usually in case of 3-dimensional topography of the surface, often thicker layers).

After bake-out of the resist (at $\sim 100^\circ\text{C}$, to remove the solvent), the dry resist is exposed. The energy entry of the particles/light causes locally a chemical change of the resist, which affects its solubility in an appropriate 'developer'.

There are two types of resist (see Fig. 6.36).

- **positive resist:** exposure with particles/light increases the solubility of the exposed parts of the resist (e.g. by breaking polymer chains). Subsequently, the exposed areas of the resist are removed in a developer.
- **negative resist:** the exposure strengthens the resist structure (e.g. by cross-linking polymer chains) and decreases the solubility. Subsequently, the non-exposed areas of the resist are removed in a developer.

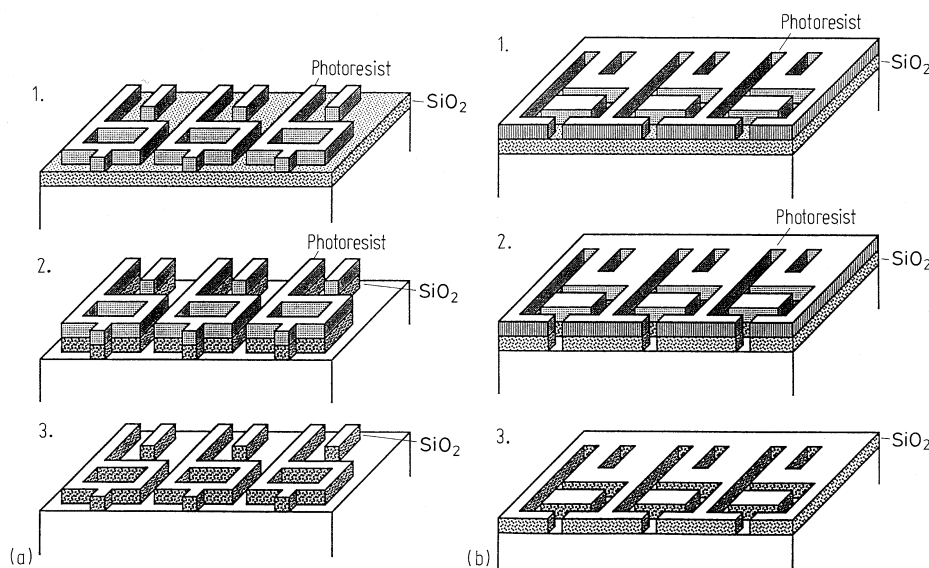


Fig. 6.36: Photolithography (for details see below) (a) with positive resist, (b) with negative resist of the same mask. The two upper panels (1.) show the resist structure (on top of a SiO_2 film) after developing. [from Bergmann-Schäfer, *Lehrbuch der Experimentalphysik, Bd. 6, Festkörper* (1992); Abb. 6.69].

a) Photolithography (optical lithography)

To define the structure that shall be realized, a layer ($\sim 1 \mu\text{m}$ thick) of a photoresist (sensitive to UV light) is coated on a wafer surface.

Subsequently, the resist is exposed through a mask (e.g. chrome structure on glass) with UV light (projection- or contact exposure in a so called *mask aligner*). The local modification of the resist material changes its solubility.

During the following developing step, the resist areas which were exposed (positive resist) or not exposed (negative resist) are removed. Hence, the desired structure (encoded in the Cr mask) is transferred into the resist (see scheme in Fig. 6.37).

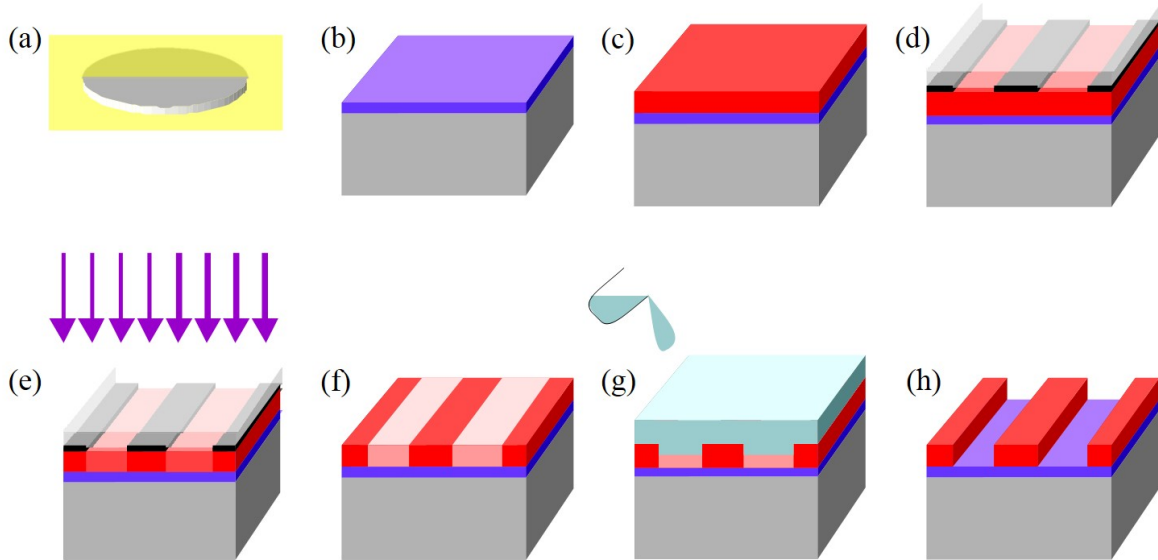


Fig. 6.37: Photolithography: (a) dicing of the substrate (optional – can also be done later), (b) modify surface if necessary, e.g. oxidize, (c) coating with resist, (d) place glass mask with Cr pattern on top of sample, (e) expose resist through Cr mask to UV light, (f) modified resist structure, (g) developing of resist structure, (h) resist structure after developing.

In optical lithography, diffraction effects are limiting minimum feature sizes to roughly half of the wavelength of the used light (several 100 nm).

Spatial resolution/smallest line width:

$$\Delta = k_1 \cdot \frac{\lambda}{NA}$$

λ : wavelength of the used light

k_1 : factor that depends on the imaging- and resist system (~ 0.4)

$NA = n \cdot \sin(\alpha)$: numerical aperture of the imaging lens with half aperture angle α in a medium with refractive index n

In order to improve the spatial resolution of photolithography, the wavelength has been steadily reduced:

- 434 nm and 365 nm with Hg vapour lamps [1970s and 1980s]
- Excimerlaser: 248 nm (KrF-laser); 193 nm (ArF-laser) [1990s until today]

Increase of the numerical aperture:

improvement from ~ 0.4 (Hg vapour lamps) to ~ 0.9 (ArF-Laser)

By optimization of various parameters and by using additional ‘tricks’, such as double exposure, the achievable minimum feature sizes with highly advanced photolithography for industrial applications in semiconductor technology were reduced to about 20 nm!

For the production of highly integrated circuits, the requirements on the cleanliness of the environment (clean room) and on the quality of the pattern transfer are tremendous.

Example:

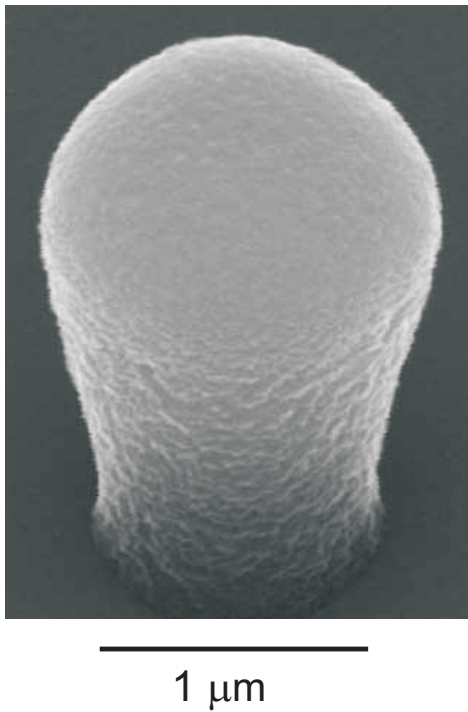


Fig. 6.38: "Final promises": via photolithography produced resist structure – actually to produce an antidot in a Nb thin film. The image shown here was taken by scanning electron microscopy (SEM). M. Kemmler, C. Gürlich, H. Pöhler; Universität Tübingen; in the FIFA world championship year 2006 [from Spiegel Online, <http://www.spiegel.de/wissenschaft/mensch/0,1518,424268,00.html>]

b) Electron beam (e-beam) lithography

For the realization of deep submicron structures, mostly in research (much less within the industrial sector), the exposure of (e-beam) resist can be done in a scanning electron microscope, or in special electron beam writers.

In this case, electron-beam-sensitive polymers – e.g. polymethylmethacrylate (PMMA) – are used for the realization of resist masks with smallest feature sizes down to $\sim 5 - 10$ nm. The smallest feature size is not limited by diffraction effects, but rather by the electron beam diameter and electron back-scattering effects (see also Sec. 3.1 on microscopy).

The e-beam is focused to ~ 1 nm spot size and is scanned over the resist surface. According to a predefined algorithm, the e-beam is switched on or off (more precisely, deflected on or off the sample surface) by a beam-blanker, such that the resist is exposed to the desired pattern. Analogous to optical lithography, e-beam-sensitive positive or negative resists can be used. Accordingly, the polymer is either decomposed by the e-beam and removed during the subsequent chemical developing step, or it is cross-linked, such that it remains as the desired pattern on the sample surface after the development step.

Advantages: very flexible in shape and positioning of the structures, very high spatial resolution, overlap of several exposure levels is possible with high accuracy

Disadvantage: very long exposure times

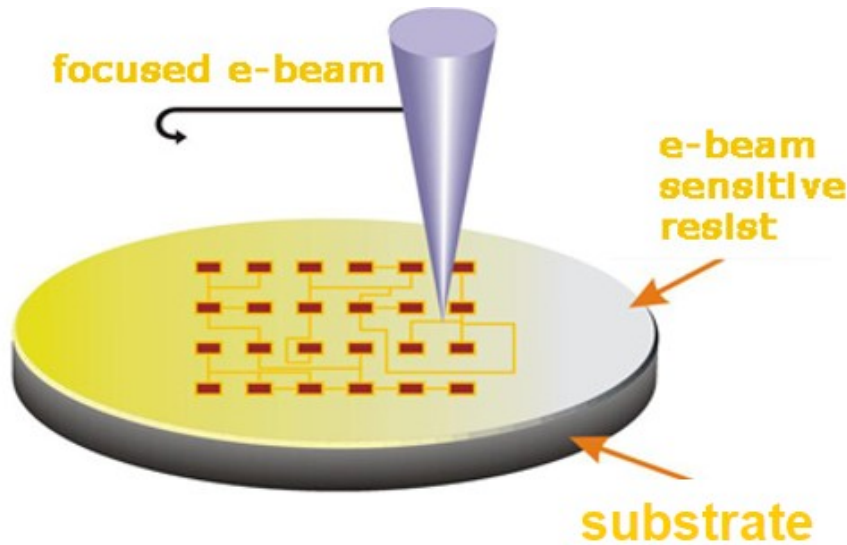


Fig. 6.39: Scheme of exposure with a focussed electron beam

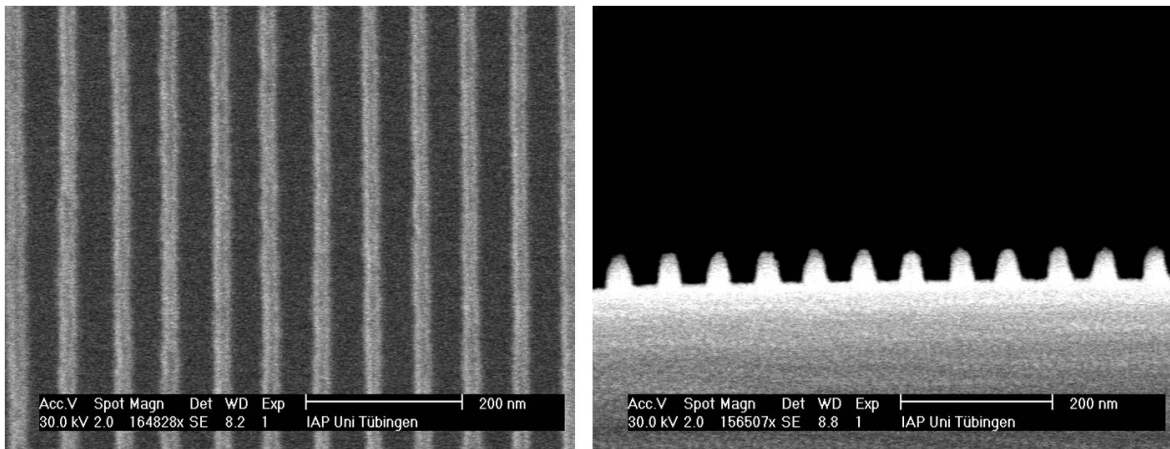


Fig. 6.40: Top and side view (SEM images) of an array of lines (60 nm period), which were produced by e-beam lithography in HSQ (Hydrogen-Silsesquioxane) negative resist [M. Häffner, Universität Tübingen (2006)]

c) Nanoimprint lithography

Nanoimprint lithography is a parallel-print procedure, which uses a master-stamp (e.g. made from silicon) for nanopatterning. The patterning of the master stamp can be done, e.g., by e-beam lithography. Hence, the smallest feature sizes that can be realized are comparable to e-beam lithography (~ 10 nm). The master-stamp is coated with a non-sticking surface, and transferred as a negative to a polymer. This produces a flexible (daughter) stamp.

In the next step a substrate is deposited with an imprint resist. The daughter stamp ('mold' in Fig. 6.41(a)) is covered with a non-sticking layer and, usually in a vacuum chamber, it is evenly pressed into the resist (Fig. 6.41(a)). In the pressed state the resist is hardened. This can be done by cooling down the resist to below its glass temperature, or it can be cross-linked with UV light. Subsequently, the daughter stamp is separated

carefully from the resist structure. The resist structure corresponds to the structure of the original master stamp. Possible resist residues inside the indentations between the structures can be removed via an oxygen plasma treatment or by etching.

Advantages of the nanoimprint lithography are the high spatial resolution and the parallel process (faster than e-beam lithography at the same resolution). The stamps can be reused many times. A disadvantage is the progressive abrasion of the stamps. There are pilot projects for large-area *roll-to-roll*-applications, however, the technique has not yet been established for industrial use. An example is shown in Fig. 6.41.

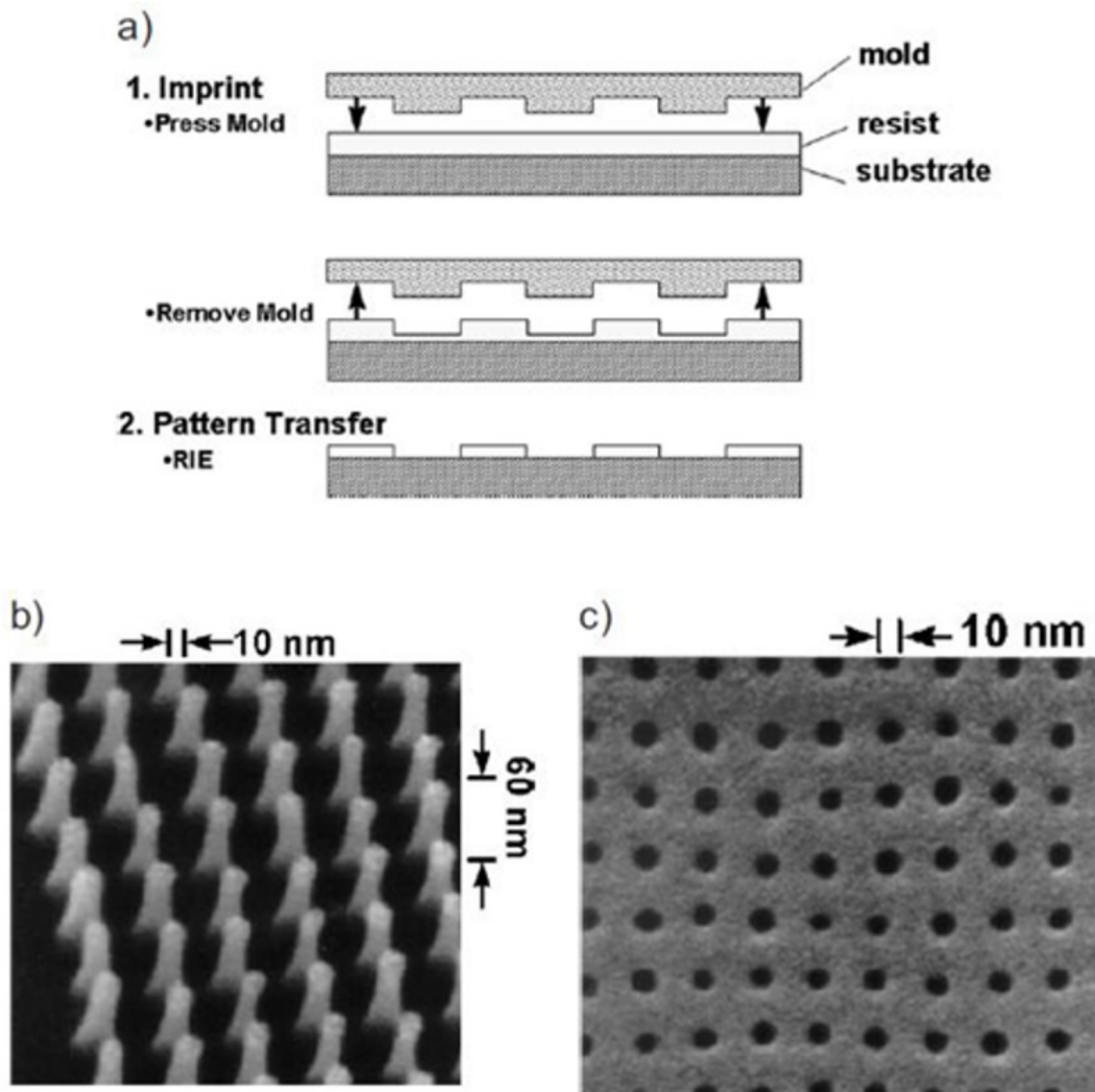


Fig. 6.41: Parallel patterning by nanoimprint lithography. a) schematic representation of the imprint process, b) SEM image of a stamp with 10 nm nano rods, c) SEM image of an imprint of the nano rod stamp into PMMA resist [from S. Y. Chou *et al.*, J. Vac. Sci. Technol. B **15**, 2897 (1997)].

6.3.2 Lift-off technique

To produce a patterned thin film, one first produces a patterned resist structure on a substrate by one of the lithography techniques as described in Sec. 6.3.1. Subsequently, the patterned resist structure is coated by the thin film, using one of the deposition processes as described in Sec. 2.2; see Fig. 6.42(i). After thin film deposition, the resist is dissolved (typically in acetone), i.e. from those areas which were covered by resist, the film grown on top of the resist is also removed; see Fig. 6.42(j).

⇒ In those areas, which were not covered by the resist, the thin film is deposited directly onto the exposed substrate regions, and the desired thin film structure remains as a permanent negative pattern of the resist mask; see Fig. 6.42(k).

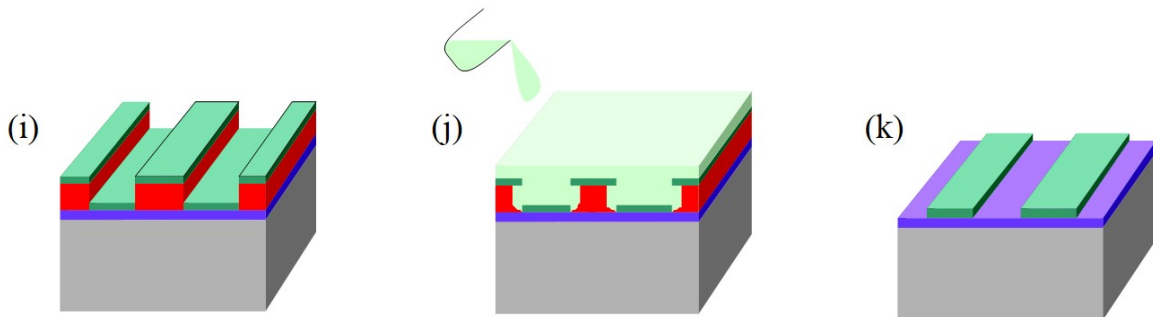


Fig. 6.42: Scheme of lift-off patterning: (i) after patterning a resist mask (red) on top of a substrate, a thin film (green) has been deposited. (j) the resist is removed in a solvent; the film grown on top of the resist is also removed. (k) resulting thin film structure on top of the substrate.

Lift-off techniques are often used to produce metallic thin film structures, which serve as electrical contacts. As the resist mask is fabricated on a substrate **before** the deposition of the film, an etching step for patterning of the thin film is avoided.

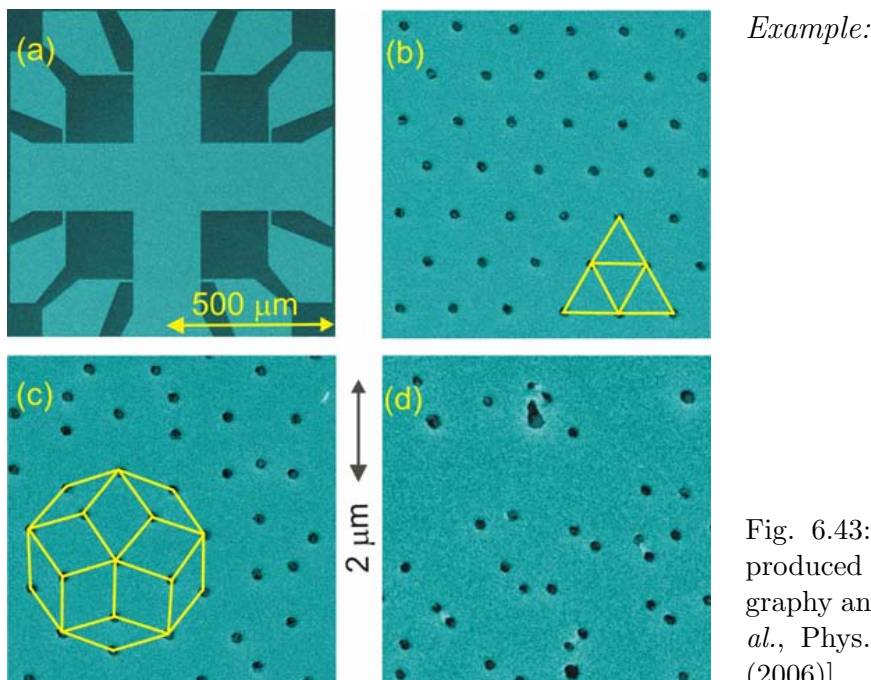


Fig. 6.43: Antidots in Nb-films, produced by electron beam lithography and lift-off [M. Kemmler *et al.*, Phys. Rev. Lett. **97**, 147003 (2006)].

6.3.3 Etching techniques

In the following we present two techniques, which are used to transfer the topography of a patterned resist structure into a thin film underneath. This is done by removing thin film areas which are not protected by the resist mask, see Fig. 6.44(i). Subsequently, the resist is removed in a solvent (typically acetone); see Fig. 6.44(j).

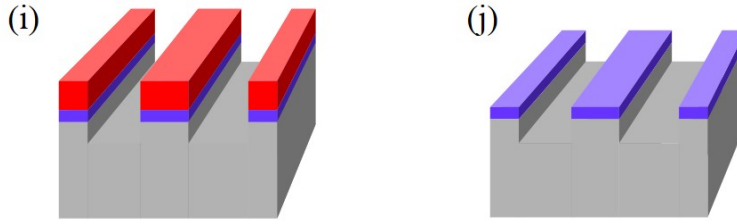


Fig. 6.44: Transfer of resist structure into thin film underneath by etching: (i) after etching; (j) after removal of the resist mask → nanostructured topography.

a) Chemical wet etching

The unprotected thin film areas are etched (removed) in acid or an alkaline solution (depending on the material).

In case of a SiO_2 layer on Si, the pattern is transferred into SiO_2 by hydrofluoric acid (HF). In case of a resist mask which is deposited directly on Si, one can use for example a potassium hydroxide solution (KOH).

Subsequently, the resist mask is dissolved or ashed in an oxygen plasma (step 4 in Fig. 6.45).

Disadvantage: isotropic etching (comparable etching rates in each direction) results in an underetching of the resist layer. Hence, the transferred feature sizes do not match the features on the mask; produces rounded edges (see Fig. 6.45(a)).

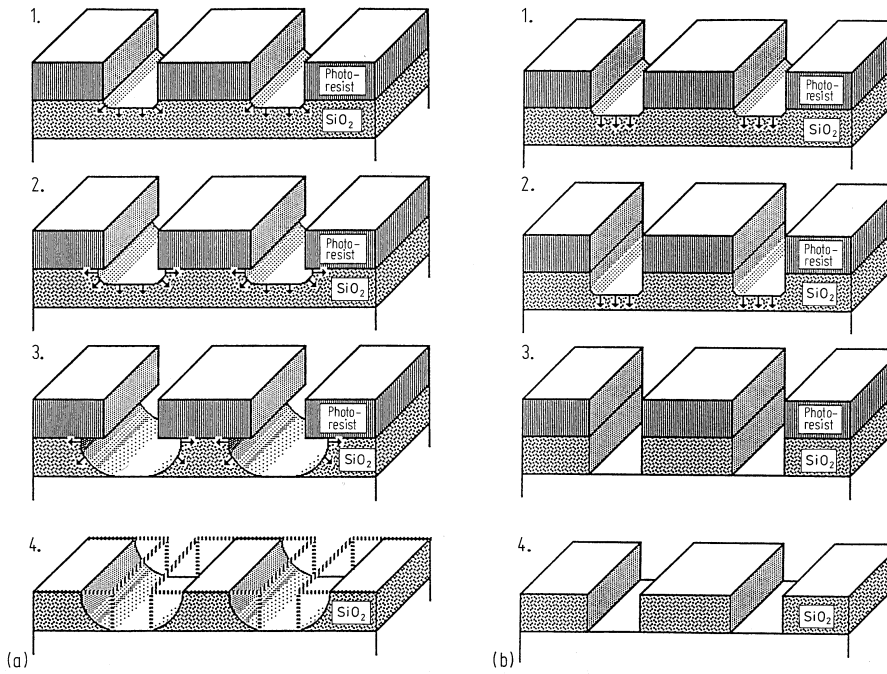


Fig. 6.45: etching processes: (a) **chemical wet etching** with isotropically attacking etching solution, (b) **dry etching** with anisotropically attacking ion beam or plasma [from Bergmann-Schäfer, *Lehrbuch der Experimentalphysik, Bd. 6, Festkörper* (1992); Abb. 6.73].

b) Dry etching

Instead of chemical wet etching, different dry etching processes can be applied.

- **physical dry etching – ion milling:**

Ablation of material by ion bombardement (usually with Ar⁺-ions)

- from directed ion beam ⇒ *ion beam etching (IBE)*,
- or in a plasma

Advantage (in contrast to chemical wet etching):

More strongly anisotropic process, which better preserves the features as defined by the resist mask (see Fig. 6.45(b)).

Disadvantages:

Less selective, i.e., different materials are removed with comparable etching rates; the ions also etch the resist mask and may also etch the layer below the material that has to be removed. Furthermore, the etching rate can vary with the angle of incidence of the ion beam or with crystal direction; this effect can produce a rough surface.

- **reactive dry etching – reactive ion etching (RIE):**

Suitable chemical reactions between the particles from a plasma (or ion beam) and the surface material that has to be etched, yield volatile reaction products. Often gaseous reactive fluorine compounds are used (SF₆, CHF₃, CF₄). During the reaction atoms are removed from the thin film surface and the volatile reaction products are drained by the vacuum pumping system.

Advantages:

- (i) The anisotropy of the etching process is adjustable (by the energy of the incoming ions), i.e. RIE is a combination of physical and chemical etching. Up to almost perpendicular walls (vertical etching rate ≪ horizontal etching rate) in the etched film can be achieved; see Fig. 6.45(b).
- (ii) The process is strongly selective, i.e. masks made from suitable material are barely attacked, while the film material to be removed can have a high etching rate. Moreover, the etching process can be stopped, when a much less reactive material underneath the film to be etched is reached.

Example: Nb reacts in an SF₆-plasma to produce volatile fluorine compounds, while an Al film below Nb is not etched. This is exploited e.g. in the patterning of Nb/Al/Nb Josephson junctions.

6.3.4 Focussed ion beam (FIB) milling

This technique is an attractive extension of IBE. Here, an ion beam is focused by appropriate beam optics to form a small (nm-sized) beam spot that can be scanned across a sample surface. This yields a highly localized milling of the sample surface, without the need of a mask. This technique is also simply called *FIB* or *Focused Ion Beam Etching (FIBE)*.

FIB systems have been developed since the 1970s and 1980s. A significant improvement of this technique came with the development of a new type of ion source:

The *Liquid Metal Ion Source (LiMIS)*, see Fig. 6.46, permits very good focusing and hence a very high ion current density, yielding sufficiently high etching rates.

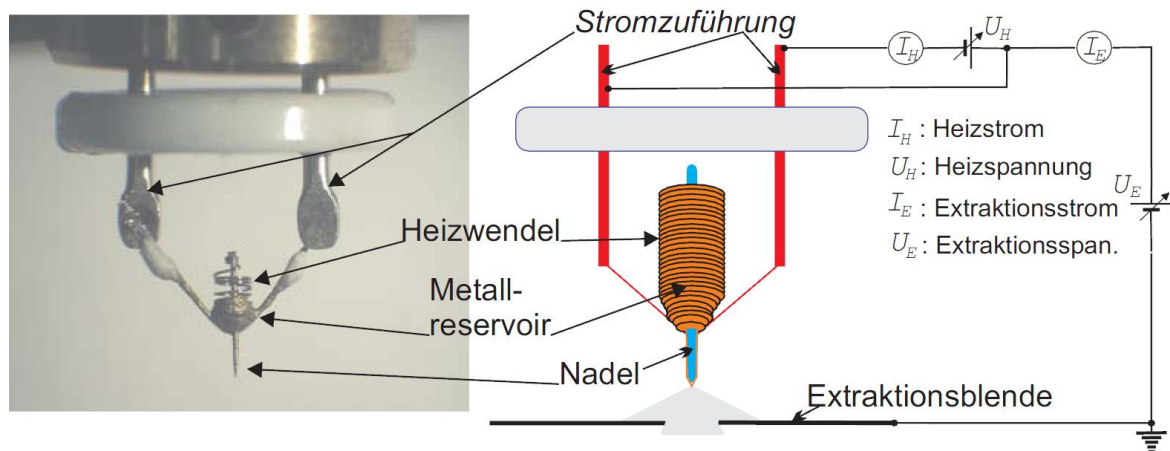


Fig. 6.46: Photograph (left) and schematic representation (right) of a LiMIS (Liquid Metal Ion Source). By heating of the spindle with the heating coil the metal gets fluid, flows to the peak of the spindle and forms a very tiny LiMIS-head due the electric field which is applied there [T. Ishitani, H. Kaga, in: Electron Microscopy 44, 331 (1995)].

The material that has to be ionized in the LiMIS (typically gallium) is located within a heated reservoir and is in contact with a needle (typically tungsten) which has a sharp tip at its bottom end. The heated liquid material from the reservoir is wetting the needle. Due to the low melting temperature and low vapour pressure, a tapered source (~ 5 nm radius) is formed at the sharp tip. Due to a very high electric field applied to the tip ($> 10^9$ V/m), field emission takes place, i.e., the material is ionized and accelerated to an extraction aperture as a beam. By far the most frequently used material for LiMIS is Ga. Alternative materials are In, Sn, Au and Bi.

The ion beam is focused by electrostatic lenses along the beam path. Since the mass of the ions is about five orders of magnitude larger than the electron mass, magnetic lenses are not applicable. For imaging the sample surface, typically secondary electron detectors or secondary ion detectors are used. Note: Surface imaging with a scanning ion microscope is of secondary importance.

Substantial strengths of FIB milling:

Highly flexible manipulation of sample surfaces; direct etching of structures into the surface by ion bombardment with a very good spatial resolution of a few nanometers – there is no need to fabricate and use a resist mask.

Disadvantages:

As a serial process, this technique is relatively slow, which yields extremely long etching times for large areas. Moreover, structures in close (lateral) vicinity to the patterned edges and the material underneath the milled areas can be significantly damaged due to amorphization or ion implantation.

Instead of etching with the ion beam (subtractive process), one can also grow nanostructures directly on a surface with a focused ion beam (additive process). This can be done by *focused ion beam induced deposition (FIBID)*. Here, precursor gas molecules, which contain the material that has to be deposited, are inserted through a nozzle near the surface. The molecules which cover the surface are separated locally into a component (e.g. Pt, or Co) which grows at the beam spot position, and a volatile component, which is removed. The molecules are separated due to the incident energy of the ion beam. One important application of FIBID is editing (shorting in combination with cutting) of circuits as a flexible means of modifying and testing a chip-layout.

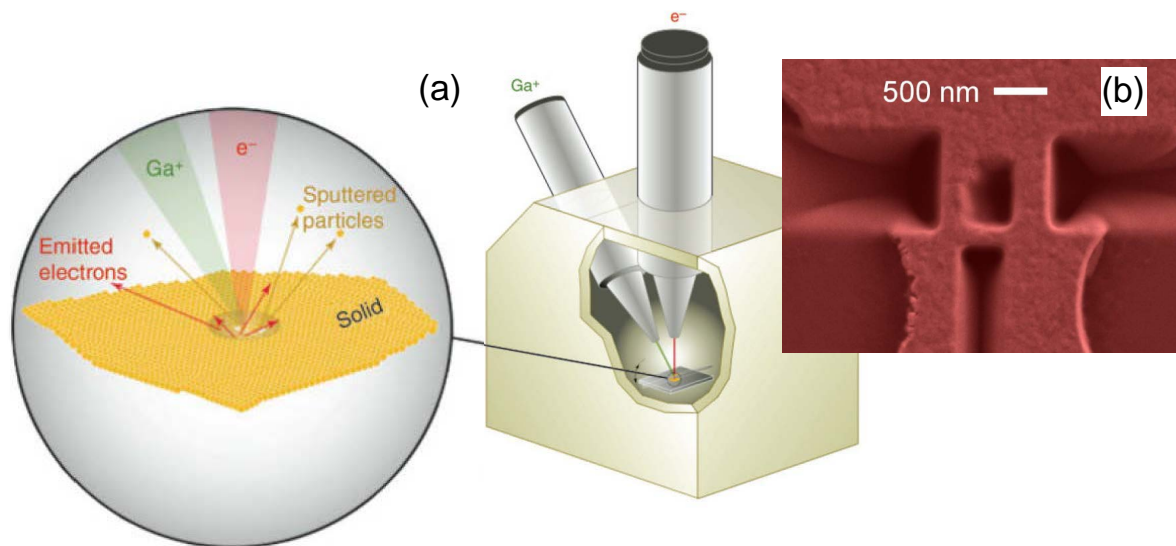


Fig. 6.47: Dual beam FIB, which combines SEM and FIB: (a) schematic view [C. A. Volkert, A. M. Minor *et al.*, Focused Ion Beam Microscopy and Micromachining. In: MRS Bulletin 32, 389 (2007); www.mrs.org/bulletin]. (b) SEM image of a $\text{YBa}_2\text{Cu}_3\text{O}_7$ (YBCO) nanoSQUID, which has been patterned by FIB [D. Koelle *et al.*, Nanotechnologie Aktuell, issue 5 (2012)].

A dual beam (or *cross beam* or *multi beam*) FIB system combines SEM with FIB; see Fig. 6.47(a). This enables FIB milling and/or FIB-induced deposition simultaneously with inspection/imaging by SEM. Figure 6.47(b) shows as an example a superconducting nanostructure (a nanoSQUID), which has been produced by Ga-FIB.

Further developments of FIB systems are driven by the requirements of the semiconductor industry, such as testing and failure analysis of highly integrated circuits (e.g. by excavating different layers on a chip).

6.3.5 Self-Assembly

During **self-assembling processes** nano-units assemble autonomously to nanostructures. These processes are driven by interactions and take place under appropriate conditions without external influence. During such processes, the free energy of the system is generally reduced.

Examples for self-assembling nanostructures:

- **Self-assembled monolayers (SAMs):** e.g. organic molecules arrange themselves to form a monolayer on a surface by chemical bonding. A typical example is the binding with thiol groups on gold surfaces. While the thiol groups bind chemically to the substrate, the molecular tails usually organize collectively to align away from the substrate at high coverage. SAMs are used to create chemically defined surfaces (inert or with specific binding properties or other features related to their surface energy determined largely by their endgroup). They can also be structured laterally.

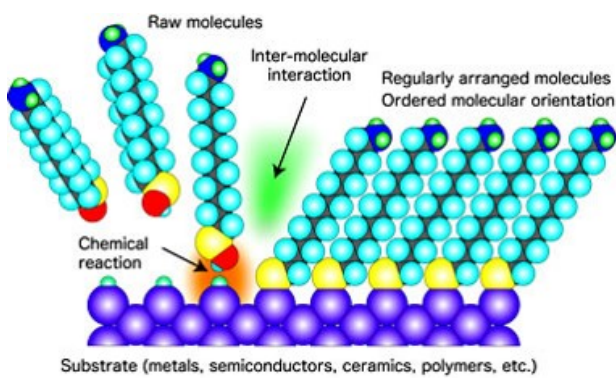


Fig. 6.48: Scheme of the formation of a monolayer from organic molecules by SAMs [http://www.mtl.kyoto-u.ac.jp/english/laboratory/nanoscopic/nanoscopic.htm]

- Wet-chemical synthesis of **colloids**: With synthesis-procedures, colloidal nanocrystals in the form of nanospheres, prisms, cubes, sticks, stars etc. are produced, e.g. from gold or silver. By optimizing the synthesis conditions (temperature, duration, concentration, reagents and surface active agents (*surfactants*)) and subsequent separation techniques, it is possible to produce monodispersive distributions with very low standard deviation. The nanocrystals are covered with molecular functionalization layers in order to stabilize them.
- **Self-assembly of nanocrystals into superstructures:** An interesting further development arises from the targeted and ordered self-assembly of the nanocrystals into superstructures. These then can contain *two* lattices, one being the atomic lattice within the nanocrystals (if these are crystalline) and the other being the arrangement of the nanocrystals, i.e. the superlattice. An overview is given in K. S. Sugi et al., Chem. Comm. **58**, 6998 (2022). The interplay between the atomic lattice and the superlattice can give rise to interesting ordering phenomena and correlations (I. A. Zaluzhnyy et al., ACS Nano Lett. **17**, 3511 (2017)).

Employing organic semiconducting molecules as ligands of the nanocrystals, if assembled under appropriate conditions these systems can be considered coupled organic-inorganic nanostructures (COINs), in which also the associated electronic transport exhibits interesting features (A. Maier et al., Adv. Materials **32**, 2002254 (2020)).

We note that the assembly of nanoparticles can also be employed to create photonic crystals, i.e. periodic arrangements of particles of typically several 100 nm in size such

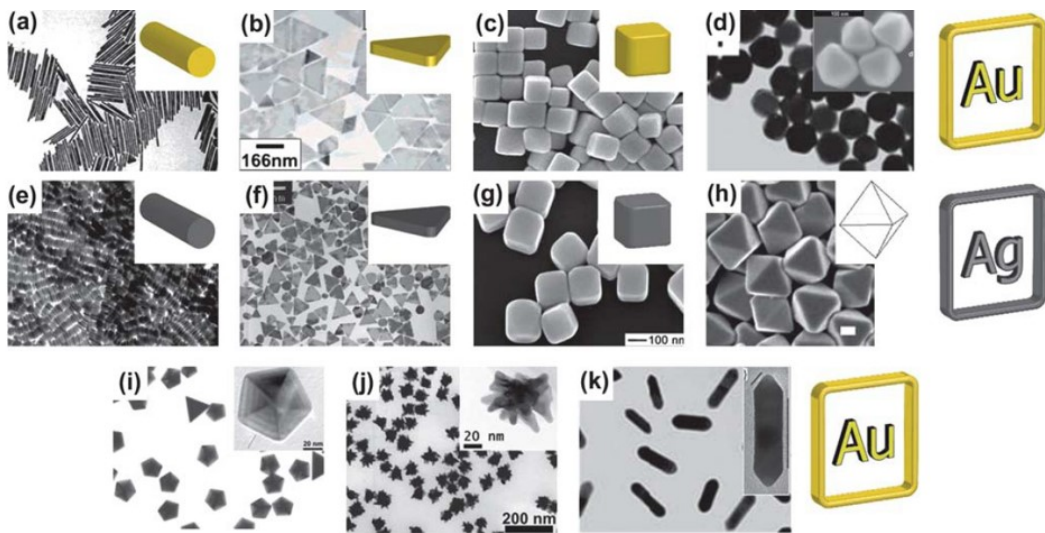


Fig. 6.49: Examples of differently formed colloidal nanocrystals [J.M. Romo-Herrera et al., Nanoscale 3, 1304 (2011)]

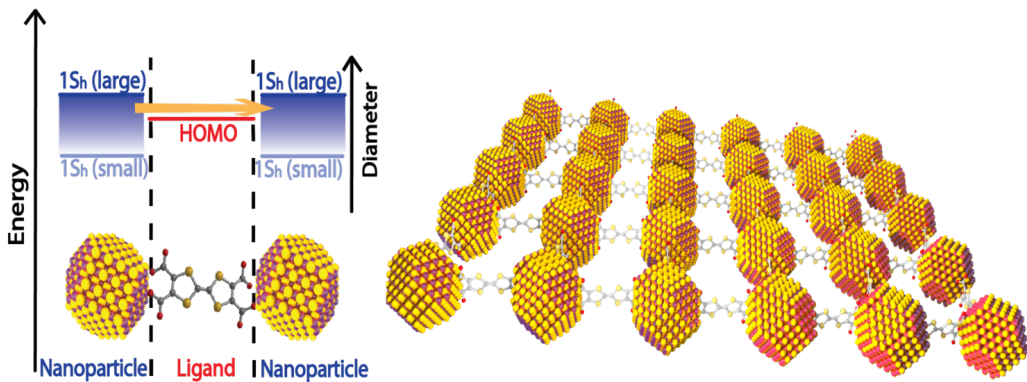


Fig. 6.50: Schematic of coupled organic-inorganic nanostructures (COINs) and their energy levels (M. Scheele et al., PCCP 17 (2015) 97)

that the spectrum resembles that of the electronic bandstructure of a conventional solid, even with a bandgap.

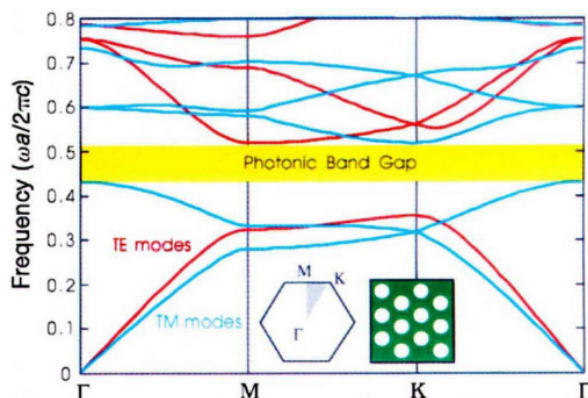


Fig. 6.51: Typical photonic bandstructure exhibiting a gap (J.D. Joannopoulos et al., Nature 386, 143 (1997))

- **Diblock-copolymers** are polymers which consist of two types of monomers. Always two monomer chains are joined to form a diblock-copolymer (e.g. PS-PMMA). Beneath a transition temperature the polymers arrange themselves periodically by attraction of monomers of the same type. This leads to the emergence of macroscopic order. According to the phase diagram (see Fig. 6.52) cylinder, blade or spherical structures are built. Along the x -axis the proportion of the monomer A is shown, and along the y -axis the "Flory-parameter" $\chi \sim (1/(k_B T))[E_{AA} + E_{BB} - 2E_{AB}]$ times the number of segments N within a copolymer chain is shown. Here, χ is a measure of the relative interaction strength of the monomers.

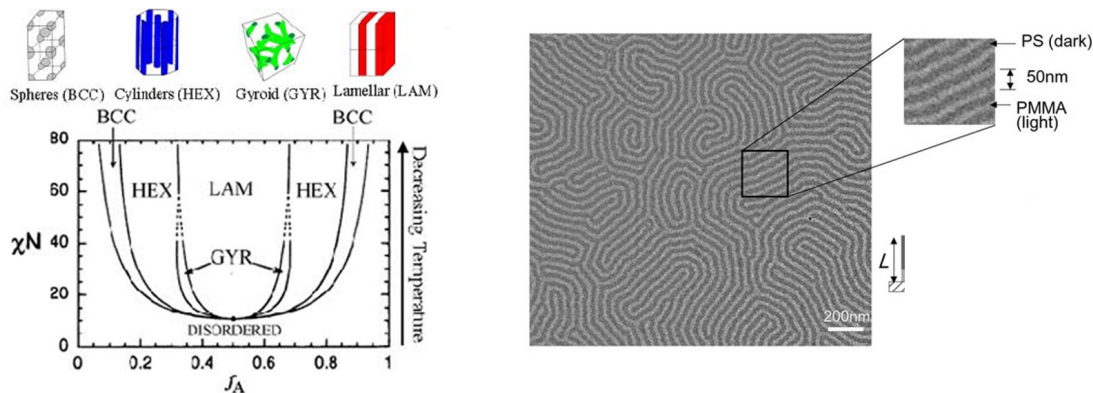


Fig. 6.52: Phase diagram of the structure formation and lamella structure from PS-b-PMMA diblock-copolymer [<http://web.mit.edu/8.334/www/grades/projects/projects10/-AlexanderPapageorge/Page6.html>; W. A. Lopes and H. M. Jaeger, Nature **414**, 735 (2001)]

- **Micelles:** From the surface active or amphiphile chemical bonds (tensides) with hydrophile and lipophile components, spherical molecular aggregates ("hedgehog structures") are built by self-aggregation. Their center can be loaded with metal salts (flexikon.doccheck.com/de/Mizelle).

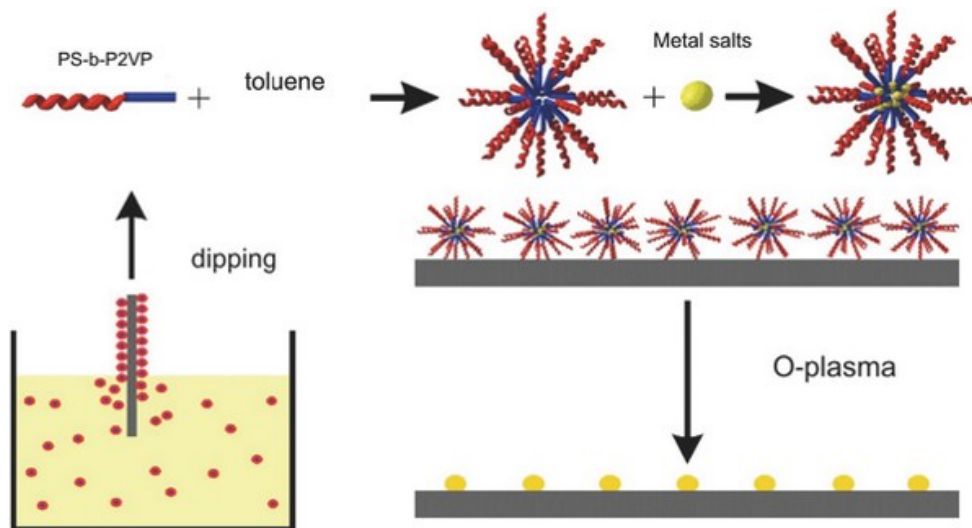


Fig. 6.53: Fabrication of FePt nanoparticles via a self-assembled layer made of micelles by *dip-coating* and *ashing* [<https://www.uni-ulm.de/en/einrichtungen/electron-microscopy-group-of-materials-science/research/materials/magnetic-nanoparticles.html?print=1>]

- **Monolayers from polystyrene-nanospheres:** polystyrene-nanospheres are deposited from solution onto surfaces. With appropriate parameters this results in large areas of hexagonally structured mono- or bilayers. The nanospheres can be reduced in size with an oxygen-plasma treatment and/or they can be used as masks for metalization or milling processes (→ **nanosphere lithography**).

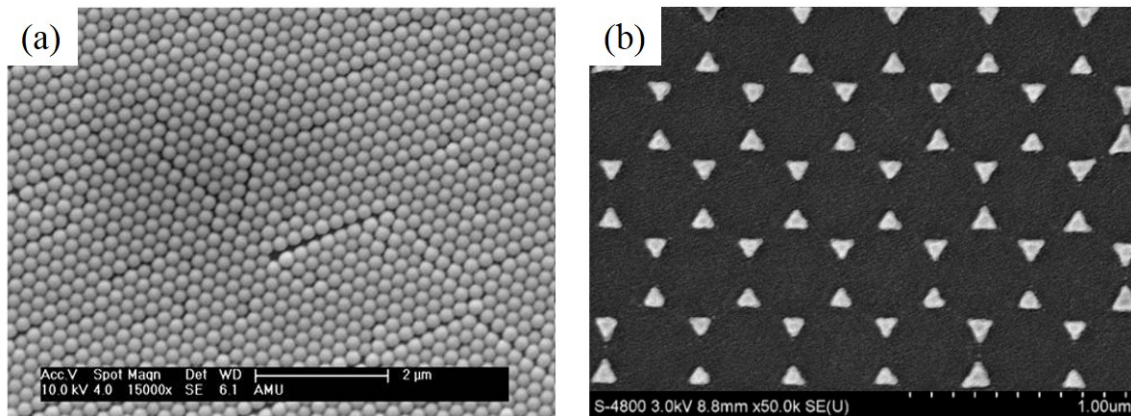


Fig. 6.54: (a) Self-assembled hexagonal monolayer composed of nanospheres (b) ordered gold-nanotriangles after deposition of the monolayer and removal of the nanospheres [AG Fleischer, Universität Tübingen]

- **DNA-origami:** DNA consists of four different bases. Single-stranded DNA combine to double helix DNA if complementary sequences of base pairs find each other. By suitable design of DNA sequences, the DNA strands form self-assembled defined two dimensional patterns. DNA-origami can be extended to the third dimension by using long single-stranded DNA-strands as *scaffolds*, and many short DNA strands as *staples*. Due to the staples the scaffold can be deformed, or additional nanoparticles such as DNA-tagged gold-colloids can be linked to the scaffold at defined positions.

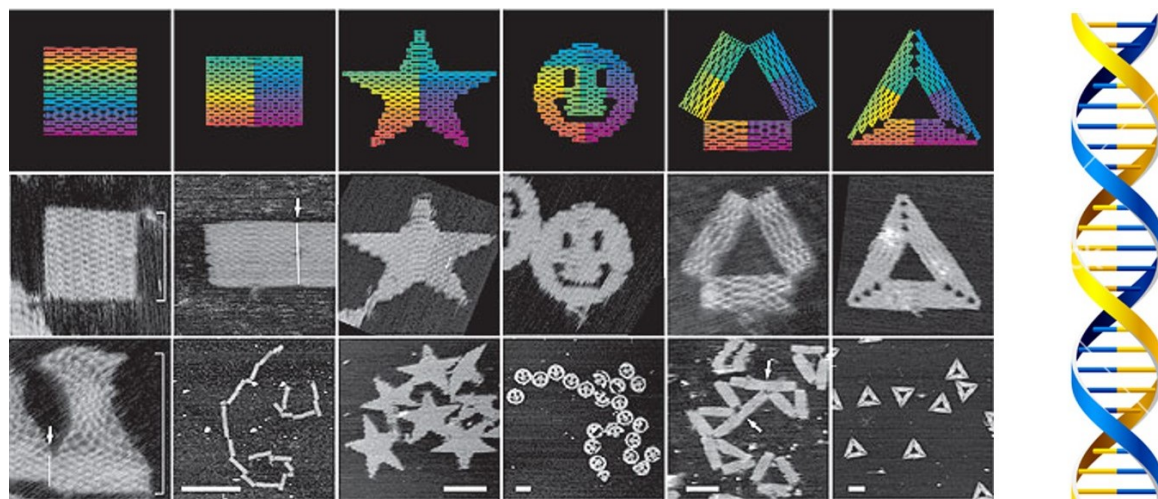


Fig. 6.55: DNA-origami; top: basepair-indices, middle and bottom row: AFM images; scale (b) 1 μm, (c-f) 100 nm [P.W.K Rothemund, Nature 440, 297 (2006)]

- **Quantum dots** from lattice mismatches in hetero-epitaxy (see Section on preparation, film growth and epitaxy). The idea is that material A grows epitaxially (i.e.

with a defined lattice relationship) on material B. If the lattice mismatch is such that A does not cover B (typically due to a too large lattice mismatch), it may form island. These islands may be just in the form of small crystals with well-defined properties and be considered quantum dots.

By combining several techniques and/or several length scales it is possible to produce **hierarchical nanostructures**. In *directed self-assembly*, e.g., boundary conditions for self-assembling are created locally. examples:

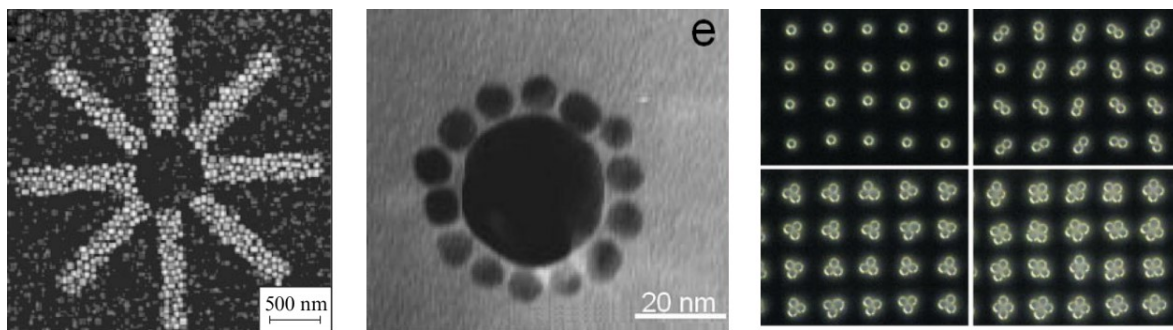


Fig. 6.56: Hierarchical nano structures [Terekhin et al., Russ. Chem. Rev. **80**, 453 (2011), Mucic et al., JACS **120**, 12674 (1998), Lee et al., Adv. Mater 14, 572 (2002)]

- **Structured arrangements on chemically modified surfaces:** The surface properties of substrates are modified locally, e.g. by making parts of the surface hydrophylic vs. hydrophobic, or by attaching specific SAMs. This way, the assembly of further components can be either promoted or prevented in a controlled way.

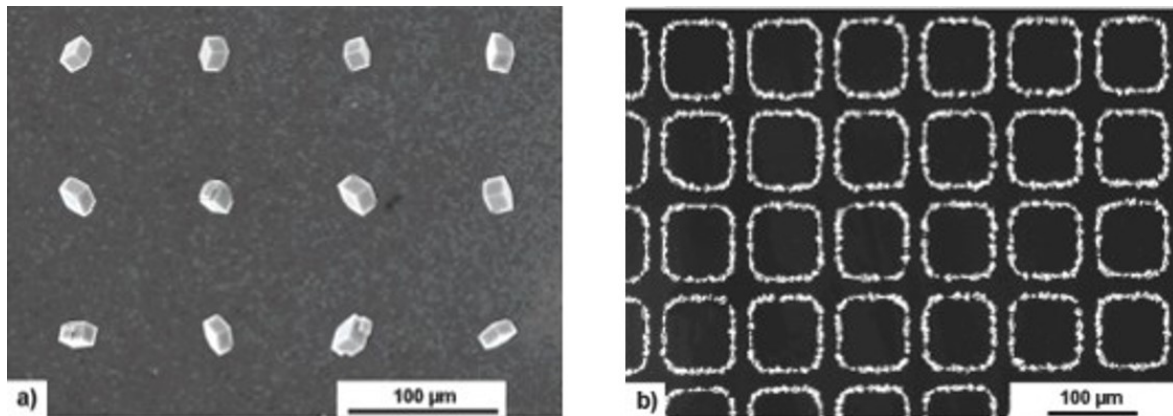


Fig. 6.57: (a) Calcite-crystals which grow selectively on the (012) plane of a micropatterned SAM on Ag(111); (b) selective calcite deposition on a SAM at the edges of an Au-Ag-surface [J.C. Love et al., Chem. Rev. **105**, 1103 (2005)]

- **Capillary Force Assembly:** A surface layer is prepatterned, for example, lithographically. The meniscus of a solution of colloid-particles is dragged over the surface. Due to capillary forces the colloids are deposited in the cavities. After the removal of the mask, defined clusters of colloids remain on the sample.

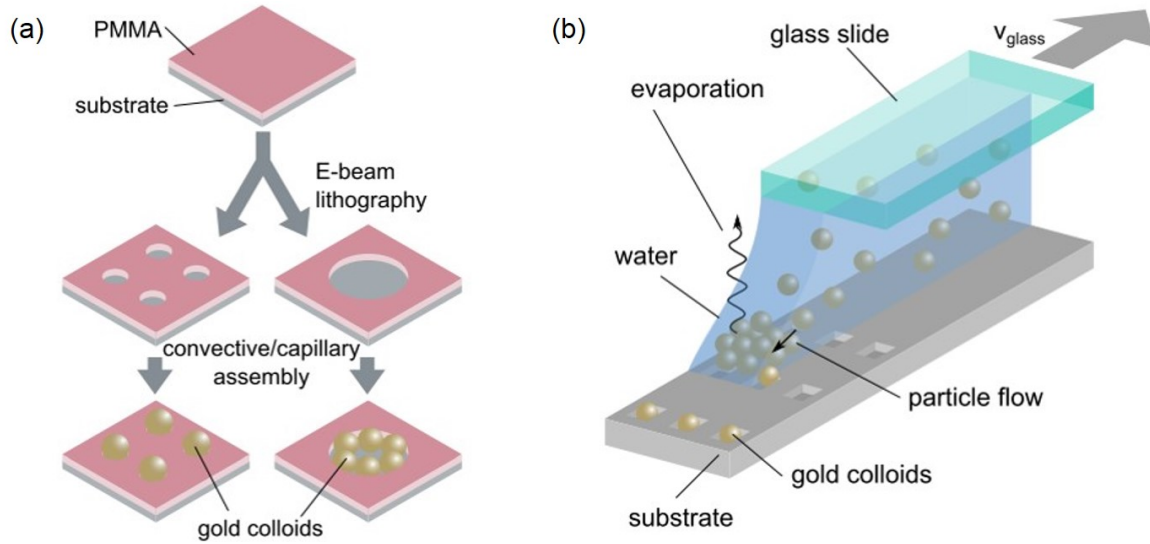


Fig. 6.58: (a) Pre patterning of a resist layer in order to deposit colloid particles, (b) scheme of the capillary force assembly [S. Dickreuter, Univ. Tübingen]

